Structural and functional roles of calcium ion in photosynthetic membrane protein complexes

Yong, Li

(Degree)
博士（農学）

(Date of Degree)
2014-03-25

(Date of Publication)
2020-03-25

(Resource Type)
doctoral thesis

(Report Number)
甲第6024号

(URL)
https://hdl.handle.net/20.500.14094/D1006024

Doctoral Dissertation

Structural and functional roles of calcium ion in photosynthetic membrane protein complexes

光合成膜蛋白質複合体におけるカルシウムイオンの構造的および機能的役割

Yong Li

Graduate School of Agricultural Science

Kobe University

January　2014

Contents

Chapter 1 General introduction

1.1 Photosynthetic organisms

Photosynthesis is the fundamental chemical reaction that takes place in photosynthetic organisms to convert light energy into chemical energy through a series of photosynthetic redox events. Photoautotrophs can synthesize hydrocarbons directly from carbon dioxide using energy of light, whereas photoheterotrophs use organic compounds, rather than carbon dioxide, as a source of carbon. The photosynthetic organisms are divided into two categories depending on the kind of electron sources. When water molecules are utilized as electron donors, oxygen molecules are produced as a by-product. This type of photosynthesis is performed by cyanobacteria, algae and higher plants, and called as oxygenic photosynthesis which have maintained the atmospheric oxygen level and allowed the evolution of living organisms using aerobic respiration. On the other hand, no oxygen molecules are evolved when hydrogen, hydrogen sulfide or organic acids are used as the electron donors. This type of photosynthesis is called as anoxygenic photosynthesis, which occurs in primitive photosynthetic bacteria such as purple bacteria, green sulfur and non-sulfur bacteria, and heliobacteria, evolved early in the history of life.

Generally, a photosynthetic charge separation takes place at the reaction centers (RC) of photosynthetic organisms utilizing light energy collected by light-harvesting (LH) complexes, and the light-induced electrons are transferred through photosynthetic electron transport pathways mediated by various cofactors. The photosynthetic RCs are classified into two groups depending on the types of electron transport system; the type-I RC containing iron-sulfur complexes in photosystem I,

green sulfur bacteria and heliobacteria, and the type-II RC containing quinone complexes in photosystem II, purple bacteria, and green non-sulfur bacteria.

1.2 Photosynthesis in type-II reaction center

Photosynthetic organisms with type-II reaction centers are evolutionally related each other since they have commonly central domains of heterodimeric protein subunits and quinone-type electron transport system. These phototrophs are, however, largely different in the protein composition and several cofactors, which are closely related to the stability of photosystems. A number of biochemical and physicochemical studies have provided valuable information on the relation between structure and stability of type-II RCs, including LH1-RC complexes from purple bacteria, and PSII from cyanobacteria and higher plants.

1.2.1 Purple bacteria

In purple photosynthetic bacteria, light energy is captured by two types of light-harvesting (LH) pigment-protein complexes, i.e. peripheral antenna LH2 and core antenna LH1 complexes, and transferred efficiently to RCs where primary charge separation of *a*-type bacteriochlorophyll (BChl-*a*) special pairs occur across the membrane [1]. Two electrons from the RC are transferred to a ubiquinone to form a ubiquinol, which migrates to a quinone pool in the membrane. The photo-oxidized special pairs of the RCs are reduced by cytochrome bc_1 complexes through soluble heme proteins to form the cyclic electron flow. Electron transport pumps protons across the membrane and the resultant trans-membrane proton motive force is used by the ATP-synthase to generate ATP (Figure 1-1).

High resolution three dimensional crystallographic structures of isolated RC complexes have been reported for both mesophilic [2, 3] and thermophilic [4] purple bacteria. The results demonstrated that RCs are comprised of four intrinsic protein subunits (C, H, M and L), but the extrinsic proteins, ubiquitous for PS II, are not involved in the assembly of the bacterial RCs. In contrast, the X-ray structure of the RC associating with the LH1 has been limited to *Rhodopseudomonas* (*Rps.*) *palustris* at moderate resolution [5]. Generally, LH1 complexes are oligomers of minimal subunits composed of α- and β-polypeptides, BChl-*a* and carotenoid molecules. The RC is surrounded by the LH1 with a one-to-one stoichiometric ratio to form LH1-RC complexes (Figure 1-2). Recent electron microscopic (EM) and atomic force microscopic (AFM) studies showed two-dimensional projection maps at low resolution (8.5 to 26 Å), indicating a variety of LH1 complexes forming 12- to 16-meric assembly of $\alpha\beta$-subunits depending on the species [6-11]. However, the LH1-RC structure at atomic resolution is absolutely required for elucidating details of the function and structure of LH1 pigment-protein complexes. Since the RC tightly associates with the LH1, interaction modes between both complexes, and the size and/or shape of LH1 rings are significant to understand the structural functional consequences, including structural stabilities, quinone transport mechanisms, and excited state dynamics of the LH1-RC complex.

The LH1 complex shows characteristic electronic absorption properties due to BChl-*a* dimers and carotenoid molecules incorporated into the $\alpha\beta$-subunits. These pigments are useful as internal probes for monitoring structural and functional properties of the LH1-RC complexes. In a typical mesophilic purple bacterium *Allochromatium (Alc.) vinosum*, the LH1 complex is suggested to have a macrocycle with a 16-fold symmetry [6]. The BChl-*a* – BChl-*a* interactions within the LH1 ring

resulted in the characteristic absorption property of the core complex as shown in Figure 1-3. The LH1-RC contains only *a*-type BChl molecule of which Q_y, Q_x and Soret bands appear at 880, 590 and 390 nm, respectively, as well as carotenoid bands around 450 – 550 nm and RC bands at 780 and 800 nm. Interestingly, thermophilic *Thermochromatium* (*Tch*.) *tepidum* showed an unusual red-shift of the LH1 Q_y peak to 915 nm along with slight red-shifts of Soret and Q_x bands although peak positions for carotenoid and RC bands remained to be unchanged [12]. The large red-shift of the Q_y band seems to be disadvantage in terms of the uphill energy transfer from the LH1 to the RC [13]. Taking into account that *Tch. tepidum* is a sole thermophile among purple bacteria, the relationship between thermostability and low-energy Q_y transition is a matter of interest.

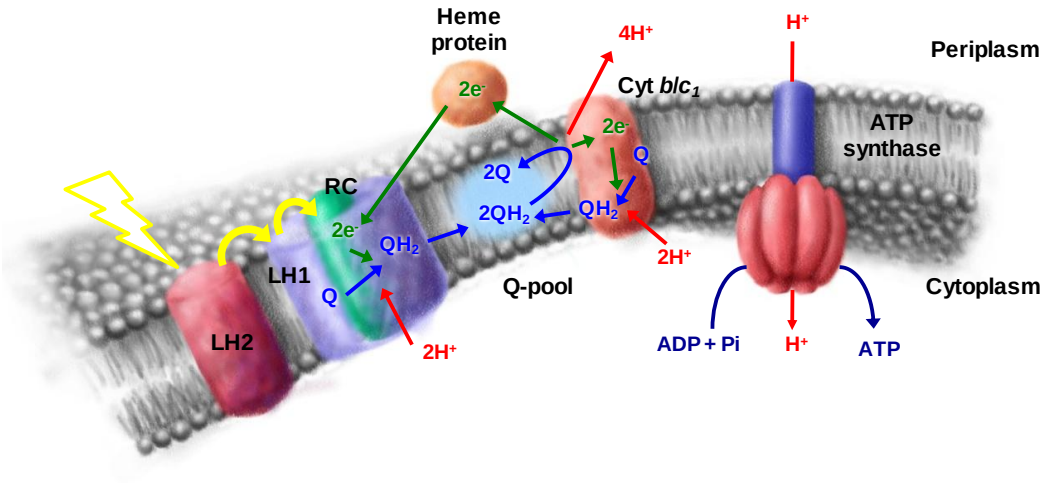

Figure 1-1. Photosynthetic apparatuses and the reaction scheme in an intracytoplasmic membrane of purple bacteria.

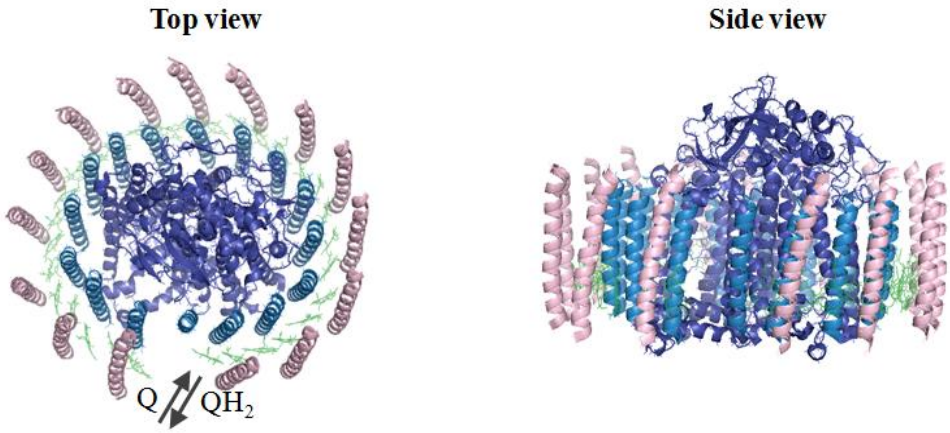

Figure 1-2. The crystallographic structure of an LH1-RC complex from *Rps. palustris* at 4.8 Å resolution [5]. The RC (purple) comprised of C, H, M, and L subunits is surrounded by the LH1 involving α- polypeptides (blue), β-polypeptides (magenta), BChl-*a* molecules (green).

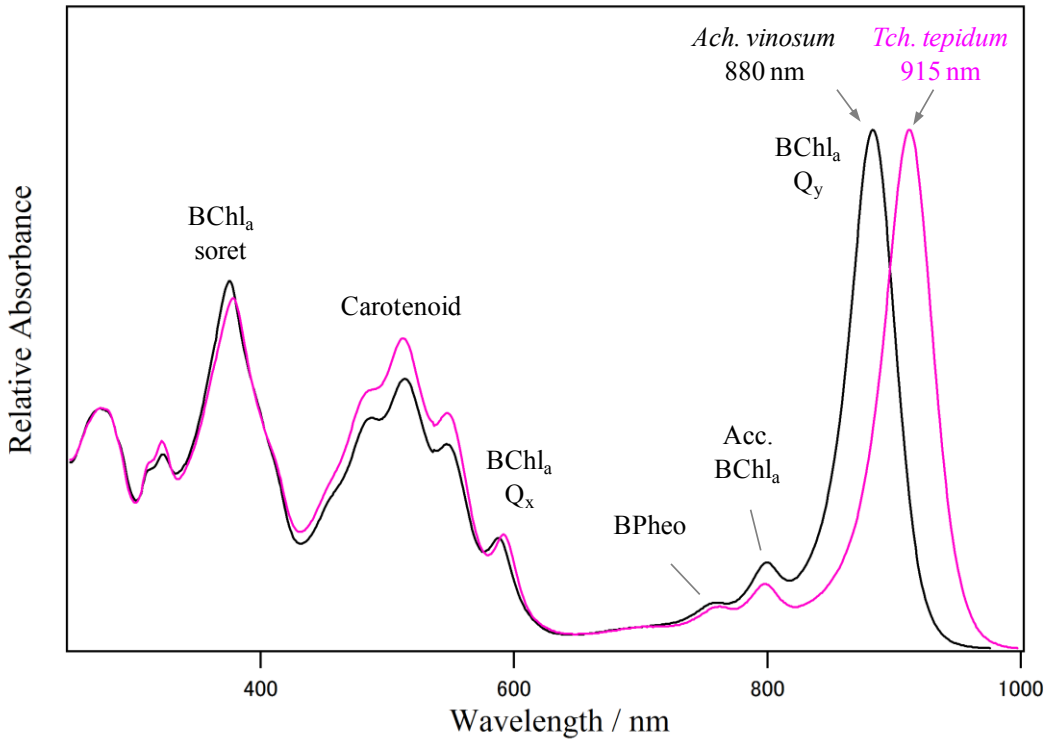

Figure 1-3. Absorption spectra of LH1-RC complexes from thermophilic *Tch. tepidum* (magenta) and mesophilic *Alc. vinosum* (black)(unpublished result).

1.2.2 Photosystem II in cyanobacteria and higher plants

Oxygenic phototrophs including cyanobacteria and higher plants convert photon energy into chemical energy through a series of light-induced electron transfer reactions initiated with the charge separation of chlorophyll special pairs located in the central part of photosystem I and II (PSI and PSII). The reducing power is transferred from PSII to PSI through cytochrome b_6f, and finally utilized for reduction of $NADP^+$ to assimilate CO_2. The oxidized equivalents accumulated on the PSII donor side are neutralized by substrate waters to release protons for driving ATP synthase and O_2 molecules as a by-product.

The photosynthetic oxygen evolution occurs in the oxygen-evolving complex (OEC) of PSII. The OEC is composed of a heterodimer of D1 (psbA) and D2 (psbD) proteins associated with two chlorophyll proteins (CP), CP47 (psbB) and CP43 (psbC), and involves a catalytic Mn_4CaO_5 cluster located on the lumenal side of PSII. These are highly conserved from cyanobacteria (Figure 1-4) to higher plants (Figure 1-5) to preserve the essential function of oxygenic phototrophs. In the past decade, X-ray crystallography has revealed the structures of cyanobacterial PSII at resolutions of 3.8 Å to 2.9 Å [14-18]. A very recent structural model at the atomic resolution level has revealed details of the ligation structure of the Mn_4CaO_5 cluster [19]. The Mn ions are bridged by several oxygen atoms and coordinated by water molecules as well as by Asp, Glu, Ala, and His residues in PsbA and/or PsbC proteins (Figure 1-6). The oxidized equivalents accumulated on the cluster and/or its ligands are reduced by electrons provided from a splitting reaction of substrate water molecules through a light-driven S-state cycle with five intermediate states S_n (n = 0 – 4), where n denotes the number of oxidizing equivalents stored (Figure 1-7). The OEC advances from the thermally stable S_1 state to the next oxidation state in a stepwise manner by absorbing

each photon and attains the highest oxidation state S_4, followed by relaxation to the lowest oxidation state S_0 concurrent with a release of one oxygen molecule [20, 21]. Two water molecules are converted to one oxygen molecule by the OEC concurrent with release of four protons although details of the water oxidation mechanism are still a matter of debate [18, 22].

In contrast, structural analysis of PSII in higher plants has been delayed due to the instability of the membrane protein complex. The visualization of plant PSII structures has been limited to electron micrographs at low resolutions [23, 24]. Yet the findings to date strongly indicate that the structure and function of the PSII core assembly are almost identical to those of its prokaryotic counterparts, except for a critical difference in the composition of extrinsic proteins, which are lacking in purple bacteria and may provide valuable insights into the evolution of photosynthetic organisms [25]. Extrinsic proteins are thought to play essential roles for stabilizing and protecting PSII cores [26]. In cyanobacteria, PsbO, PsbV, and PsbU residing on the lumenal side of PSII play significant roles in the regulation and stabilization of the water oxidation machinery. Higher plants possess major nuclear gene-encoded extrinsic proteins named PsbO, PsbP, and PsbQ. PsbO is a common extrinsic protein highly conserved among the oxygenic phototrophs. PsbP and PsbQ indigenous to plant PSII have been proposed as the functional equivalents of PsbV and PsbU, respectively, in bacterial PSII, having replaced them during the course of evolution from ancestral cyanobacteria to higher plants. These proteins play a key role for maintaining oxygen-evolving activity at physiological rates [26, 27]. PsbO independently associates with the PSII core [28, 29], whereas binding of PsbP occurred through electrostatic interactions with PsbO [30, 31]. PsbQ requires both PsbO and PsbP for its binding [29, 30]. PsbP protein is related to the stability of the

Mn_4CaO_5 cluster [32] as well as the binding affinity of functional Ca^{2+} and Cl^- ions [33, 34]. In addition, *psbP*-deletion mutants revealed that PsbP is indispensable for the normal PSII function in higher plants [35]. Another function of this protein was indicated that PsbP has a Mn^{2+}-binding ability as a reservoir to keep or deliver manganese ions [36]. PsbQ protein is related to be binding of Cl ions [37]. Studies on transgenic tobacco [35] and Arabidopsis [38] revealed that PsbQ protein is not necessary under normal growth condition [35, 38] but is required for photoautotrophic growth under low-light condition [38].

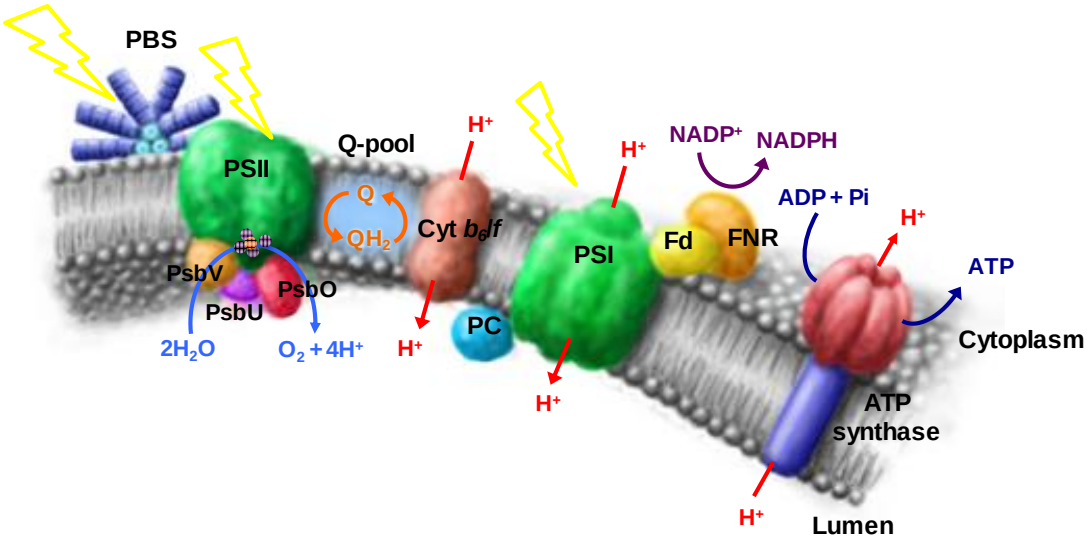

Figure 1-4. Photosynthetic apparatuses and the reaction scheme in a thylakoid membrane of cyanobacteria.

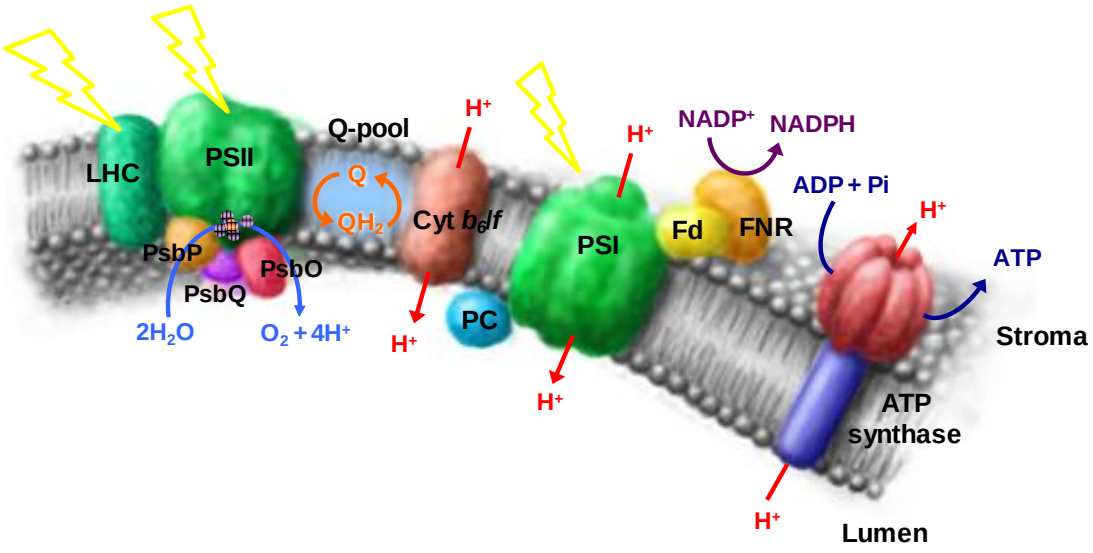

Figure 1-5. Photosynthetic apparatuses and the reaction scheme in a thylakoid membrane of higher plants.

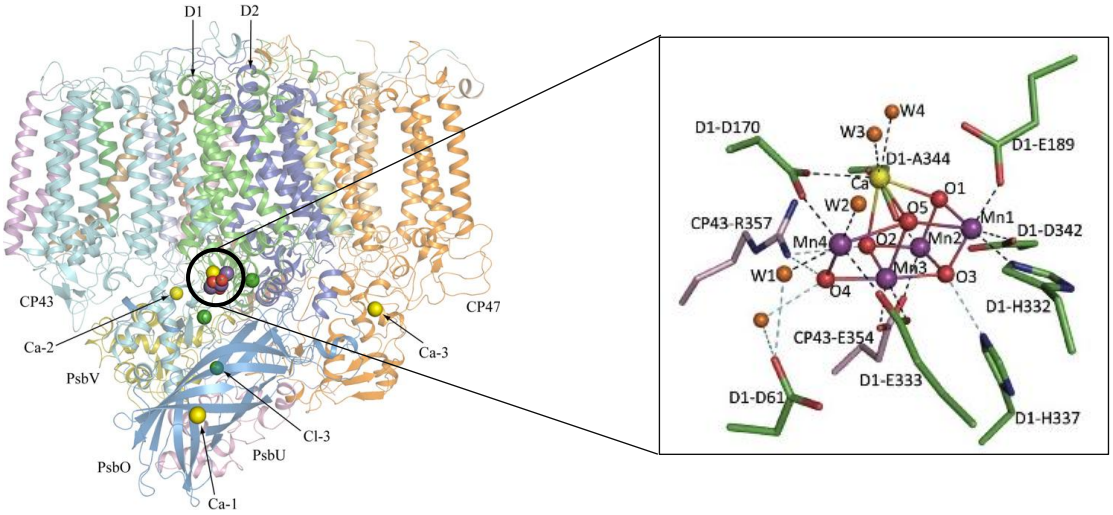

Figure 1-6. The crystallographic structure of PSII from *Thermosynechococcus vulcanus*. The inset shows an expanded view of the Mn_4CaO_5 cluster [19, 39].

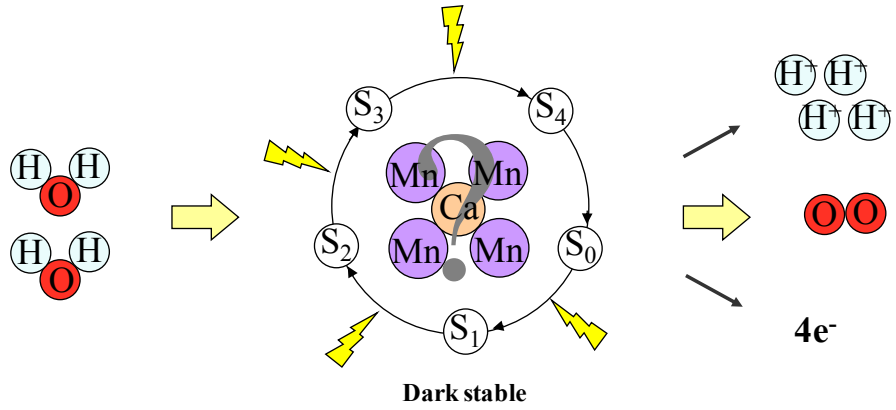

Figure 1-7. Photosynthetic water oxidation by the Kok cycle through five intermediate state (labeled S_0 to S_4) of the Mn_4CaO_5 cluster.

1.3 Roles of calcium ions in type-II reaction centers

Calcium ion is an essential nutrient playing structural roles in the cell wall and membranes and functional roles as an intracellular messenger coordinating responses to developmental signals and environmental changes in living organisms. This is true for phototrophs with type-II reaction centers, however, other intriguing and important roles of calcium ions have been reported. In *Tch. tepidum*, Ca ions are closely related to the enhanced thermal stability and unusual spectroscopic properties of the LH1-RC complexes [12, 40]. Since *Tch. tepidum* was isolated from a living environment rich in the mineral calcium carbonate, it is presumed that this bacterium uses Ca ions to enhance its heat tolerance and thereby to survive in extreme environments. After the removal of Ca^{2+} from the *Tch. tepidum* LH1-RC, the thermal stability was significantly reduced, along with unusual Q_y blue-shifts from 915 nm to 880 nm that is comparable to those in the mesophilic counterparts. The modified properties are fully reversed upon the reconstitution of Ca^{2+}. Interestingly, only strontium ion is biosynthetically replaceable with Ca ion, resulting in different spectroscopic and thermodynamic properties of the LH1-RC complexes [41]. These results support that Ca ions play key roles in stabilizing the pigment-protein assembly and modulating the light-harvesting properties of the *Tch*. *tepidum* LH1-RC complex [42]. Based on the primary sequence of the *Tch*. *tepidum* LH1 complex [43], putative Ca^{2+} binding sites are the *C*-terminal region of α-polypeptide or the *N*-terminal region of β-polypeptide, where several neighboring acidic residues are located (Figure 1-8). A recent topological study strongly indicated the location of the binding site to be at the *C*-terminal region of the $\alpha\beta$-subunit [44]. However, the structural changes of the LH1-RC proteins induced by the Ca^{2+}-binding are not detected and the molecular mechanism enhancing the thermal stability is largely unknown.

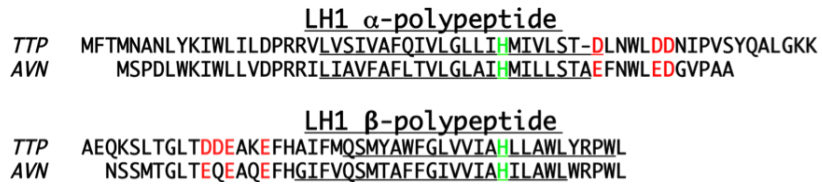

Figure 1-8. Amino acid sequences of LH1 α- and β-polypeptides from *Tch. tepidum* and *Alc. vinosum*. (Red: acidic residues forming putative metal binding sites. Green: BChl-*a* binding site.)

In the PSII of cyanobacteria and higher plants, calcium ion is an indispensable inorganic cofactor necessary for the photosynthetic water oxidation [45]. Previous studies demonstrated that O_2-evolving capabilities of the PSII were lost upon the depletion of Ca^{2+} ions, but restored by the replacement with Ca^{2+}, or to a lesser extent, with Sr^{2+}. In the absence of Ca^{2+}, the OEC can be oxidized to the S_2-state but further oxidation steps beyond the S_2-state are interrupted [46, 47]. Therefore, Ca^{2+} ions are considered as an indispensable inorganic cofactor for O_2-evolution. It has been believed that Sr^{2+} is functionally replaceable with Ca^{2+} [48] although EPR studies for the Sr^{2+}-substituted OEC revealed that magnetic properties of the Mn_4CaO_5 cluster was significantly altered [46, 47, 49].

A ^{113}Cd-NMR study demonstrated the proximity of the Mn_4CaO_5 cluster to the ^{113}Cd-bound Ca^{2+}-site, in which $^{113}Cd^{2+}$ is located in a symmetrical six-coordinate sphere of oxygen and nitrogen or chlorine [50]. In addition, EPR studies on the Mn^{2+}-supplemented PS II membranes indicated that the Mn^{2+} ion that occupies the Ca^{2+}-site is located outside the first coordination sphere of the Mn_4CaO_5 cluster [51]. Furthermore, site-directed mutagenesis studies of *Synechocystis* PCC6803 have demonstrated that mutants at Asp-59 and Asp-61 in the A-B loop of the D1 protein require higher Ca^{2+} concentrations in the culture medium for photoautotrophic growth, suggesting that these residues are involved in the Ca^{2+}-binding [52, 53]. These results indicated that the Ca^{2+} ion is located at the periphery of the Mn_4CaO_5 cluster, rather than the inside of the cluster. However, the latest high-resolution X-ray crystallographic structure of the PSII from *T. vulcanus* demonstrated that one PSII involves 4 Ca^{2+} ions [19, 39], one of which is incorporated into the Mn_4CaO_5 cluster, and the other 3 Ca^{2+} ions are loosely bound to outside of the coordination sphere [39]. Findings to date strongly indicate that Ca^{2+} ions are bound to the extrinsic proteins,

PsbO [27, 33, 54-59], PsbP [33, 36], and PsbV [60-64]. Therefore, it is still a matter of debate which Ca^{2+} ion plays the key role in the reaction mechanism for the photosynthetic water oxidation.

Chapter 2 Analysis of molecular mechanism for the enhanced thermal stability of Light-harvesting 1 reaction center complexes from the thermophilic purple sulfur bacterium *Thermochromatium tepidum*

2.1 Introduction

Purple photosynthetic bacteria capture the light energy with antenna apparatuses (LH1 and LH2) complexes and transfer the energy into an RC to initiate a charge separation and the subsequent photosynthetic redox events [1]. An X-ray crystallographic study [5] and scanning probe microscopic analyses [6, 8-10, 65] on mesophilic purple bacteria have demonstrated that the RC is surrounded by a cylindrical LH1 to form an LH1-RC complex. However, the diffraction data for the LH1-RC complexes have been limited to moderate resolutions, and details of the interaction mode between RC and LH1 complexes and the roles of the LH1 complex are not fully understood.

Thermochromatium tepidum (*Tch. tepidum*) is a thermophilic purple sulfur bacterium [66, 67]. The growth temperature is the highest (up to 58˚C) among purple bacteria, and the LH1 Q_y band appears at 915 nm, which is red-shifted unusually (~35 nm) compared to those of the mesophilic counterparts. Based on the primary sequence of the LH1 $\alpha\beta$-subunit [43] and structural information of the RC [4], it was proposed that the electrostatic interactions between acidic residues at the C-terminal region of the LH1 α-polypeptides and four basic residues specific for the *Tch*. *tepidum* RC may be responsible for the unusual spectroscopic and thermodynamic properties of this thermophilic organism [4, 68, 69]. Recently, we demonstrated that Ca^{2+} ions play a key role in the unique properties of the *Tch. tepidum* LH1-RC complexes [12, 40]. Among all known purple bacteria, only the *Tch*. *tepidum* LH1-RC complex exhibits Ca^{2+}-dependent thermal stability and spectral changes of BChl-*a* molecules bound to

the LH1 complex. When Ca^{2+} ions were depleted from the native LH1-RC complex, the Q_y peak at 915 nm was blue-shifted to 880 nm with marked deterioration of the thermal stability. The modified properties of the *Tch. tepidum* LH1-RC complex were almost completely restored after reconstitution with Ca^{2+} or, to a lesser extent, with Sr^{2+} and Ba^{2+}, but the addition of Cd^{2+} scarcely changed the properties [12, 40]. Based on the topological analysis, a putative Ca^{2+}-binding site was expected to exist at the C-terminal region of the LH1 α-polypeptides [70]. However, these results were mostly obtained by monitoring the Q_y absorption of LH1 BChl-*a* molecules, and little information is available on the structural change of the LH1-RC protein upon the metal-substitution, which is essential to clarify the molecular mechanism responsible for how the *Tch. tepidum* LH1-RC complex enhances the thermal stability by utilizing Ca^{2+}.

Fourier transform infrared (FTIR) spectroscopy is a powerful tool to monitor subtle changes in molecular structures and chemical reactions that are essential to understand structure-function relationships of biomolecules [71]. In the recent years, perfusion-induced attenuated total reflection (ATR) FTIR spectroscopy has been used to monitor the fine structural changes of proteins upon the binding of ligands, substrates, and cofactors to nicotinic acetylcholine receptor [72, 73], transhydrogenase [74], halorhodopsin [71], cytochromes c [76] and *c* oxidase [77, 78], and V-ATPace [79], or upon the redox changes and/or state transitions between intermediates of cytochrome *c* oxidase [80-83], and photosystems I and II [84, 85]. As for purple bacteria, the redox-linked structural and/or conformational changes were reported for the cytochrome bc_1 complex of *Rhodobacter* (*Rba.*) *capsulatus* [86] and the RC complexes of *Rba. sphaeroides*, *Rps. viridis* [84] and *Tch. tepidum* [87]. Apart from the perfusion-induced ATR-FTIR investigations, a recent typical ATR-FTIR study

[88] reported reduced conformational flexibility of the *Tch. tepidum* LH1-RC complex upon the binding of Ca^{2+}. However, the spectra could only provide information concerning a macro change between the Ca^{2+}- and Mn^{2+}-bound forms, and the fine structural modifications of the LH1-RC proteins induced by metal exchanges have not been detected. Here, I report for the first time metal-sensitive fine structural changes of protein backbones and amino acid side chains in the highly purified LH1 and LH-RC complexes from *Tch. tepidum* by means of perfusion-induced ATR–FTIR spectroscopy. Possible assignments for the metal-sensitive ATR-FTIR signals and its relevance to the molecular mechanism enhancing the thermal stability of *Tch. tepidum* LH1-RC proteins are discussed based on the recent structural information on the Ca^{2+}-binding site.

2.2 Materials and methods

2.2.1 Sample preparation

LH1-RC complexes from *Tch. tepidum* were purified as described previously [41] with slight modifications. Briefly, *Tch. tepidum* cells cultured at 48–50˚C for 7–10 days were disrupted in 20 mM Tris-HCl buffer (pH 8.5) at 0˚C by sonication (Sonopuls HD3200, Bandelin). The resulting chromatophores were treated with 0.32–0.35% (w/v) lauryldimethylamine *N*-oxide (Anatrace) at 25°C for 60 min followed by ultracentrifugation to remove a large portion of the LH2 complexes. The pellets were further treated with 0.9% (w/v) *n*-octyl-*β*-D-glucopyranoside (Anatrace) at 25°C for 60 min to extract the LH1-RC crudes. After ultracentrifugation, the supernatant was loaded onto a DEAE anion-exchange column (Toyopearl 650S, TOSOH) equilibrated at 4°C with 20 mM Tris-HCl buffer (pH 7.5) containing 0.08% (w/v) dodecylphosphocoline (DDPC, Anatrace). Upon a linear gradient of $CaCl_2$ concentration from 0 mM to 25 mM, I isolated for the first time the LH1 complex lacking the RC at 7~10 mM, and then the typical LH1-RC complex at ~20 mM. Sample fractions with a ratio of A_{915}/A_{280} over 3.0 for LH1 complexes and A_{915}/A_{280} over 2.1 for LH1-RC complexes were collected. The purity of the LH1 and LH1-RC complexes were confirmed by SDS-PAGE on a 12-22% gradient gel stained with CBB and sucrose density gradient centrifugation under a 10-40% (w/v) continuous gradient of sucrose concentration in a buffer containing 20 mM Tris-HCl (pH 7.5) and 0.08% (w/v) DDPC. Purification of *Allochromatium* (*Alc.*) *vinosum* LH1-RC complexes was conducted as described previously[42], and fractions with a ratio of A_{884}/A_{280} over 2.0 were collected.

The LH1 or LH1-RC fractions were concentrated with Amicon Ultra 100K filters (Millipore), and diluted 10-fold with buffer A (20 mM Tris-HCl, 20 mM $CaCl_2$,

pH7.5), and ultracentrifuged at 195,000×g for 10 min. The resulting pellet was suspended in buffer A containing 0.008% DDPC to be ~100 μM of LH1-RC complex, and used in the ATR-FTIR measurements.

Uniform ^{15}N- or ^{13}C-isotope labeling of the *Tch. tepidum* cells was performed in a medium containing $^{15}NH_4Cl$ (Masstrace Inc., 99 atom% ^{15}N) or $^{13}CH_3{}^{13}COOH$ and $NaH^{13}CO_3$ (Masstrace Inc., 99 atom% ^{13}C) as the nitrogen or carbon source.

2.2.2 ATR-FTIR Measurements

The ATR-FTIR measurement system was constructed as described in the literature by Rich and Breton [72] with modifications (Figure 2-1). FTIR spectra were recorded on a Prestige-21 spectrophotometer (Shimadzu) equipped with a mercury-cadmium-telluride (MCT) detector (Shimadzu) and a DuraSamplIR II ATR accessory with a three-bounce silicon microprism (Smiths Detection). A silicon long-pass filter was placed in front of the detector to improve the S/N ratio. An aliquot of the LH1-RC sample solution (5 μl) was deposited on the Si/ZnSe ATR prism and dehydrated for 5 min under a stream of dry nitrogen gas. Upon this dehydration, no spectral change of the LH1-RC complex was confirmed. Then, a flow-attachment consisting of a transparent acrylic plate and a rubber O-ring was laid over the sample film and connected to a peristaltic pump (MP-1000-H EYELA) via silicon tubing. Background spectra were measured after a perfusion of Ca^{2+}-buffer (20 mM Tris-HCl, 25 mM NaCl, 20 mM $CaCl_2$, pH 7.5) at a flow rate of 1 ml/min for 30 min. The buffer was switched to Sr^{2+}-buffer (20 mM Tris-HCl, 25 mM NaCl, 20 mM $SrCl_2$, pH 7.5) at a flow rate of 1 ml/min for 20 min, and the sample spectra were recorded to yield a perfusion-induced Sr^{2+}/Ca^{2+} ATR-FTIR difference spectrum. In a similar manner, Ca^{2+}/Sr^{2+} difference spectra were obtained by switching back from

Sr^{2+}-buffer to Ca^{2+}-buffer. In some cases, $BaCl_2$ or $CdCl_2$ was used instead of $SrCl_2$. Each spectrum was accumulated at 25˚C for 1.5 min (150 scans), and 30–40 spectra (4500–6000 scans) from different samples were averaged to improve the S/N ratio.

For deuterium substitution, LH1-RC samples were suspended in D_2O-buffer (20 mM Tris-DCl, 20 mM $CaCl_2$, 0.008% DDPC, pD 7.5) and incubated at 4˚C for 12 hr. Then, spectral changes upon metal-exchanges in D_2O-buffer were examined. ^{44}Ca-isotope labeling was performed using $^{44}Ca^{2+}$-buffer including 20 mM Tris-HCl, 25 mM NaCl, 20 mM $^{44}CaCl_2$ (98.7 atom% ^{44}Ca, Oak Ridge National Laboratory) at pH 7.5.

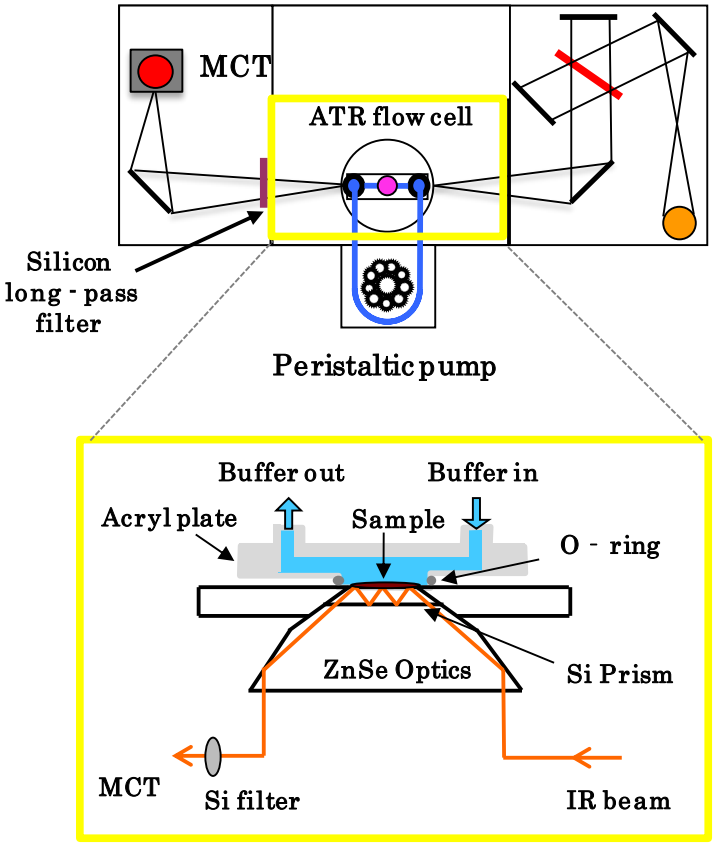

Figure 2-1. A schematic representation of the perfusion-induced ATR-FTIR measurement system. The ZnSe ATR optics with a 3 bounce silicon microprism was incorporated into the FTIR instrument and connected to a flow-attachment and peristaltic pump. A silicon long-pass filter was placed in front of the detector to improve the S/N ratio.

2.3 Results and discussion

2.3.1 Metal-sensitive structural changes in the *Tch. tepidum* LH1-RC complex

Figure 2-2 shows ATR-FTIR absorption spectra of the *Tch. tepidum* LH1-RC complex. The spectrum of the LH1-RC suspension basically exhibited only the H–O–H bending mode of water molecules at ~1640 cm^{-1}. Upon drying with a stream of N_2 gas, the film showed the characteristic amide I band (the C=O stretch of backbone polypeptides) at 1653 cm^{-1}, and amide II band (the NH bend coupled with the C–N stretch of backbone polypeptides) at 1543 cm^{-1} together with additional mid-to-low intensity bands originating from buffer components. After the rehydration of the dried film with Ca^{2+}-buffer (20 mM Tris-HCl, 25 mM NaCl, 20 mM $CaCl_2$, pH 7.5), the amplitude of the protein bands was slightly decreased but stabilized rapidly. As reported previously [72], extensive removal of detergents from the starting material was required to obtain the stable background of a sample spectrum under a buffer flow. We confirmed that the absorption spectrum of the redydrated LH1-RC film was little degraded during the measurement.

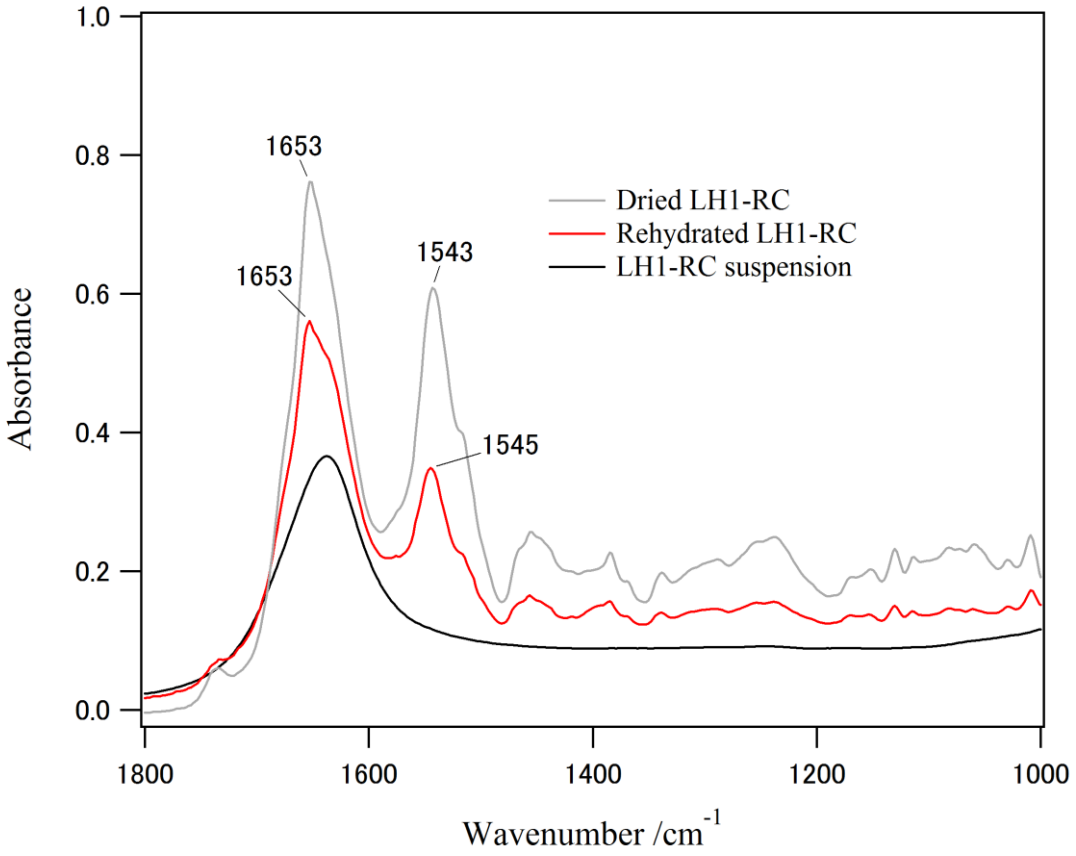

Figure 2-2. Absorption spectra of the LH1-RC complexes from *Tch. tepidum*. An aliquot of the LH1-RC suspension (black) was dried (gray) under a stream of N_2 gas, and rehydrated (red) by the perfusion of the buffer.

Figure 2-3 shows the Sr^{2+}/Ca^{2+} ATR-FTIR difference spectrum of the LH1-RC complex from *Tch. tepidum* (a, magenta). Compared to the difference spectrum without the metal exchange (c), characteristic difference bands were clearly observed in the amide I (νC=O, 1700–1600 cm^{-1}) and amide II (νC–N and δN–H, 1600−1500 cm^{-1}) regions of the polypeptide main chains upon the exchange from Ca^{2+} to Sr^{2+}. In addition, the difference spectrum may include specific vibrational modes of several amino acid side chains that interact directly and/or indirectly with the metal cations [73]. Interestingly, the characteristic bands in the Sr^{2+}/Ca^{2+} difference spectrum were observed in the subsequent Ca^{2+}/Sr^{2+} difference spectrum (black) with almost identical intensities but inverse signs. The symmetric features in both difference spectra were reproduced in the second and third cycle of the metal exchanges (data not shown), supporting the structural modifications of the LH1-RC complex induced by the metal exchange being fully reversible. In contrast, similar metal-sensitive ATR-FTIR signals were not detected in the LH1-RC complex from the mesophilic counterpart, *Alc. vinosum* (b), although several unassignable bands appeared faintly upon the metal exchange. These results demonstrate that most the ATR-FTIR difference bands are derived from unique structural modifications in the *Tch. tepidum* LH1-RC proteins upon the metal replacement, and not due to nonspecific changes in the proteins, detergents, or buffer molecules. In previous studies, metal-dependent property changes of the *Tch. tepidum* LH1-RC complexes were assessed spectroscopically by monitoring the electronic absorption [12] and emission [74], (magnetic) circular dichroism [12, 75], and (pre)resonance Raman scattering [42, 74] of BChl-*a* molecules bound to the LH1 $\alpha\beta$-subunits. Although an isothermal titration calorimetry analysis of the *Tch. tepidum* LH1-RC complex indicated exothermic conformational changes due to the binding of Ca^{2+} to the proteins [40], no significant

modification in the secondary structure has been detected in far-UV CD spectra [12]. Therefore, this is the first evidence for the detection of metal-sensitive fine structural changes in the *Tch. tepidum* LH1-RC proteins. Taking into account the metal-dependent property changes in the thermal stability of this complex [40], the present results strongly indicate that metal-sensitive ATR-FTIR bands reflect structural changes that are intimately related with the enhanced thermal stability of the LH1-RC complex from this thermophile.

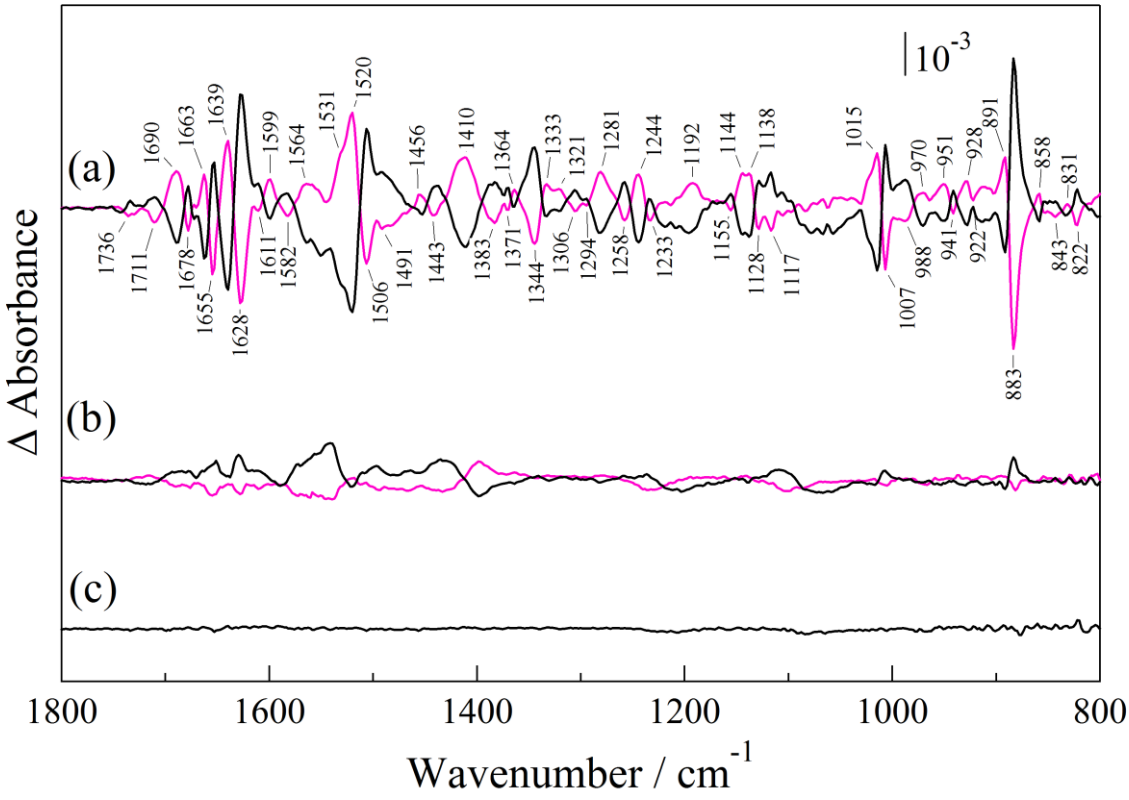

Figure 2-3. ATR-FTIR difference spectra of the LH1-RC complexes from *Tch. tepidum* (a) and *Alc. vinosum* (b) induced by switching from Ca^{2+}-buffer to Sr^{2+}-buffer (Sr^{2+}/Ca^{2+} difference spectrum, magenta) followed by switching from Sr^{2+}-buffer to Ca^{2+}-buffer (Ca^{2+}/Sr^{2+} difference spectrum, black). The difference spectrum of the *Tch. tepidum* LH1-RC complex without buffer switching (c) is presented to show the noise level.

2.3.2 Characterization of the LH1 complex lacking the RC

In contrast to the RC and LH1-RC complexes, the LH1 complex lacking the RC has not been isolated from *Tch. tepidum* yet. In the present study, we purified and characterized the LH1 complex to identify whether the observed vibrational modes originate from the LH1 or RC complex. Figure 2-4 shows the absorption spectra of LH1 (red) and LH1-RC (black) complexes isolated from *Tch. tepidum*. The absorption bands typical of BChl-*a* molecules were comparably observed at 378, 592, and 914 nm in both LH1 and LH1-RC spectra. However, small but significant differences were clearly observed in the band intensities of BPheo-*a*, the accessory BChl-*a*, and the special pair from the RC [76] at ~760, ~800, and ~880 nm, respectively, and the intensities of the bands lower than 450 nm were significantly decreased (Figure 2-4). Consequently, the ratio of Abs_{915}/Abs_{280} showing the criteria for the purity of the complexes was larger than 3. The results demonstrate that the purified LH1 complex maintains its native structure even when it is not associated with the RC.

Next, the LH1 complex was characterized using perfusion-induced ATR-FTIR spectroscopy. Figure 2-5 shows the Sr^{2+}/Ca^{2+} (a) and Ca^{2+}/Sr^{2+} (b) difference spectra of the LH1 (cyan) and LH1-RC (black) complexes from *Tch. tepidum*. Most of the bands were largely coincident between the LH1 and LH1-RC spectra in terms of peak position and intensity although faint differences due to nonspecific changes in the background intensities seemed to be involved. This result demonstrates that the metal-sensitive FTIR signals of the *Tch. tepidum* LH1-RC complex are mostly attributable to structural modifications of the LH1 proteins and the contribution of the RC is negligible under the present experimental conditions.

It is of note that the intensities of difference bands induced by metal exchanges seem to be much larger in the *Tch. tepidum* LH1-RC complex compared with those in

the other protein [77]. This may be attributed to the larger number of Ca^{2+}-binding site in the LH1-RC protein since the LH1 is proposed to be 16-mer of the $\alpha\beta$-subunit, each of which has a putative Ca^{2+}-binding site at the C-terminal region [12].

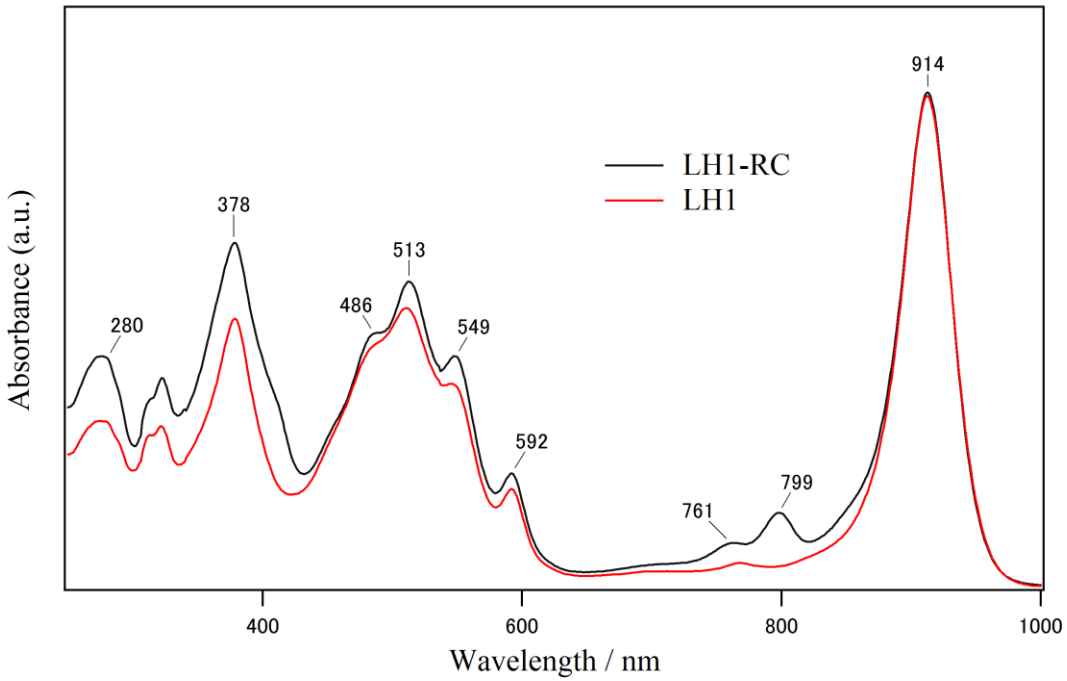

Figure 2-4. Absorption spectra of the LH1 (red) and LH1-RC (black) complexes from *Tch. tepidum*. Both spectra were normalized with respect to the Q_y maximum at 914 nm.

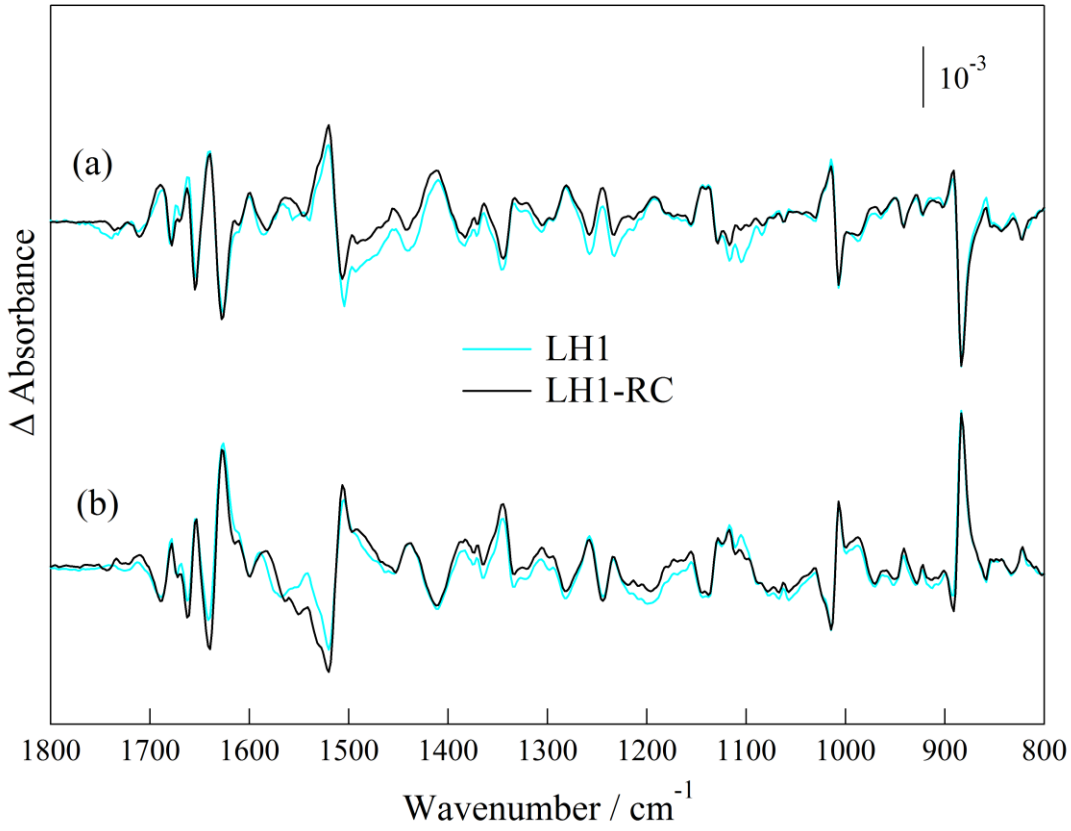

Figure 2-5. Sr^{2+}/Ca^{2+} (a) and Ca^{2+}/Sr^{2+} (b) difference spectra of the LH1 (cyan) and LH1-RC (black) complexes from *Tch. tepidum*. All spectra were normalized with respect to the 891/883 cm^{-1} differential band.

2.3.3 Properties of the Putative Ca^{2+}-binding Site and its Relevance to the Enhanced Thermal Stability of the *Tch. tepidum* LH1-RC Complexes

The previous study demonstrated that the thermal stability of the *Tch. tepidum* LH1-RC complex largely depends on the metal cation species [40]. Thus, the effects of Ba^{2+}- or Cd^{2+}-substitution for Ca^{2+} were also examined. Figure 2-6A shows the perfusion-induced ATR-FTIR difference spectra of the LH1-RC complexes from *Tch. tepidum* obtained by switching from Ca^{2+}-buffer to Sr^{2+}-buffer (a, magenta), Ba^{2+}-buffer (b, green), or Cd^{2+}-buffer (c, purple) along with their respective reversed spectra (black lines). All metal substitutions produced reversible difference spectra, which indicates that metal-sensitive structural changes are fully interconvertible even if Ba^{2+} and Cd^{2+} were employed instead of Sr^{2+}. The Ba^{2+}/Ca^{2+} (Ca^{2+}/Ba^{2+}) difference spectra were almost identical to Sr^{2+}/Ca^{2+} (Ca^{2+}/Sr^{2+}) difference spectra in terms of peak positions and band intensities as clearly seen in the double difference spectra (Figure 2-6B), which were obtained by subtracting Sr^{2+}/Ca^{2+} from Ba^{2+}/Ca^{2+} difference spectra (a) or by subtracting Ca^{2+}/Sr^{2+} from Ca^{2+}/Ba^{2+} difference spectra (b). In contrast, Cd^{2+}/Ca^{2+} (Ca^{2+}/Cd^{2+}) difference spectra (Figure 2-6A) showed markedly different spectral features, particularly in the 1750–1350 cm^{-1} region. Figure 2-6B shows the double difference spectra between Cd^{2+}/Ca^{2+} and Sr^{2+}/Ca^{2+} differences (c) or Ca^{2+}/Cd^{2+} and Ca^{2+}/Sr^{2+} differences (d). The double difference bands are prominent at 1653 and 1541 cm^{-1}, and to a lesser extent, at 1703, 1609, 1582, 1520, 1429, and 1396 cm^{-1}. These results strongly indicate that Cd^{2+}-substitution induced unique structural modifications in the vicinity of the Ca^{2+}-binding site of the LH1 proteins compared with the Sr^{2+}- or Ba^{2+}-substitutions. Interestingly, the unusual spectral changes by the Cd^{2+}-substitution were also confirmed in aqueous solutions of metal acetate complexes $M(CH_3COO)_2$ (M=Ca, Sr, Ba, or Cd), which are the simple model

compounds for carboxylates ligating metal cations (Figure 2-7A). All the spectra in panel A exhibited the asymmetric and symmetric COO^- stretching bands at ~1551 cm^{-1} and ~1416 cm^{-1}, respectively. However, their peak positions and band intensities were altered depending on the metal cations (panel B). The Cd^{2+}/Sr^{2+} (Sr^{2+}/Cd^{2+}) difference spectra exhibited clear differences at 1566, 1441, and 1412 cm^{-1} in contrast to the small changes in the Ba^{2+}/Sr^{2+} (Sr^{2+}/Ba^{2+}) difference spectra. These results are largely compatible with the present ATR-FTIR double difference spectra (Figure 2-6B), supporting the idea that carboxylate stretching bands of the metal-carboxylate complexes are sensitive to the binding property of the metal cation rather than the ionic radius. Furthermore, the spectral shapes in the symmetric COO^- stretching regions in Figure 2-6B (1429/1396 cm^{-1}) are similar with those in Figure 2-7B (1441/1412 cm^{-1}) although the peak positions were deviated by 12-16 cm^{-1}. Therefore, a possible assignment for the 1429/1396 cm^{-1} bands in Figure 2-6B is the symmetric carboxylate stretching bands, and the 1653 and 1541 cm^{-1} bands are amide I and II of the polypeptide main chain. If this is the case, Cd^{2+} may form a bidentate ligation rather than a unidentate ligation judging from the upshift of the symmetric carboxylate stretching bands from 1396 to 1429 cm^{-1}. This change modifies the specific interactions between α- and β-polypeptides at the C-terminus, leading to the destabilization of the LH1-RC complexes upon the binding of Cd^{2+}. Alternatively, an exchange of the ligation partner might occur in the vicinity of the Ca^{2+}-binding site upon the Cd^{2+} substitution since Cd^{2+} prefers softer bases as ligand partners due to their relatively weak Lewis–acids property.

The previous studies have shown that the thermal stability of the Cd^{2+}-substituted LH1-RC complex was strongly decreased to 23.8% compared with those of the LH1-RC complex reconstituted with Ca^{2+} (89.3%) or replaced with Sr^{2+}

(72.0%) and Ba^{2+} (73.2%) [40] despite the fact that Cd^{2+}-, Sr^{2+}-, and Ba^{2+}-bound forms exhibited Q_y peaks at similar positions (887–889 nm) [12]. Therefore, the unique structural changes induced by Cd^{2+}-substitution may exert little influence on any interactions that modulate the Q_y absorption properties but are intimately related with the marked deterioration of the thermal stability in the Cd^{2+}-substituted LH1-RC complexes.

It is notable that metal-sensitive ATR-FTIR signals were not apparent in the *Alc. vinosum* LH1-RC complex (Figure 2-3) under the present condition even though this complex also possesses a cluster of acidic residues in the C-terminal region in analogy with *Tch. tepidum* (Figure 2-8). A possible factor to interpret the difference of the metal requirement between both species is a deletion at the +7 position of the LH1 α-polypeptide from *Tch. tepidum*. This deletion has been suggested to be indispensable to form the coordination sphere of Ca^{2+}. Interestingly, the quite similar sequences including the deletion were confirmed in strain 970 [78] and *Trv. winogradskyi* [79]. However, these species grow at ambient temperatures, and thus, the presence of the deletion alone would not directly verify the enhanced thermal stability of the *Tch. tepidum* LH1-RC complex. Therefore, it is speculative that the presence of the deletion at the +7 position of the LH1 α-polypeptide is a necessary requirement to form a suitable Ca^{2+}-affinity site, and that the Ca^{2+}-binding induces a key conformational change of the C-terminal amino acid residues of LH α- and/or β-polypeptides.

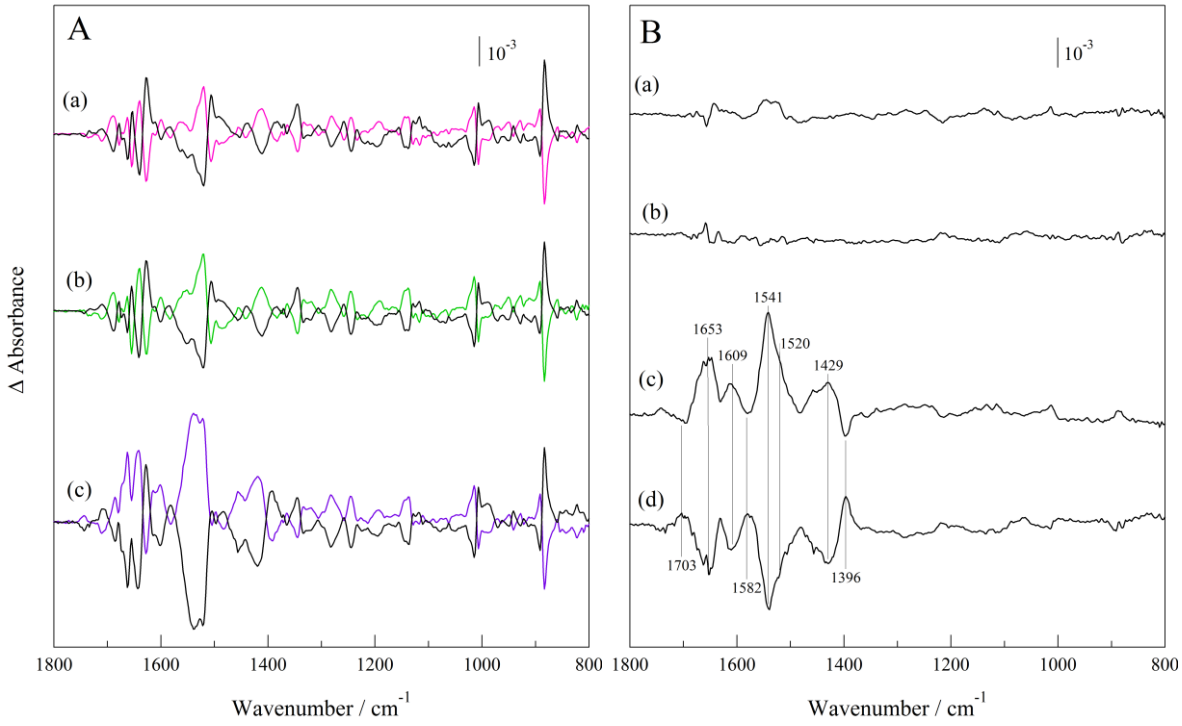

Figure 2-6. (A) ATR-FTIR difference spectra of the LH1-RC complexes from *Tch. tepidum* for the Sr^{2+}/Ca^{2+} (a, magenta), Ba^{2+}/Ca^{2+} (b, green), and Cd^{2+}/Ca^{2+} (c, purple) exchanges and their respective ensuing Ca^{2+}/Sr^{2+} (a, black), Ca^{2+}/Ba^{2+} (b, black), and Ca^{2+}/Cd^{2+} (c, black) exchanges. (B) Double difference spectra obtained by subtracting the Ca^{2+}/Sr^{2+} spectrum from the Ca^{2+}/Ba^{2+} spectrum (a), the Sr^{2+}/Ca^{2+} spectrum from the Ba^{2+}/Ca^{2+} spectrum (b), the Ca^{2+}/Sr^{2+} spectrum from the Ca^{2+}/Cd^{2+} spectrum (c), and the Sr^{2+}/Ca^{2+} spectrum from the Cd^{2+}/Ca^{2+} spectrum (d). All spectra were normalized with respect to the 891/883 cm^{-1} differential band.

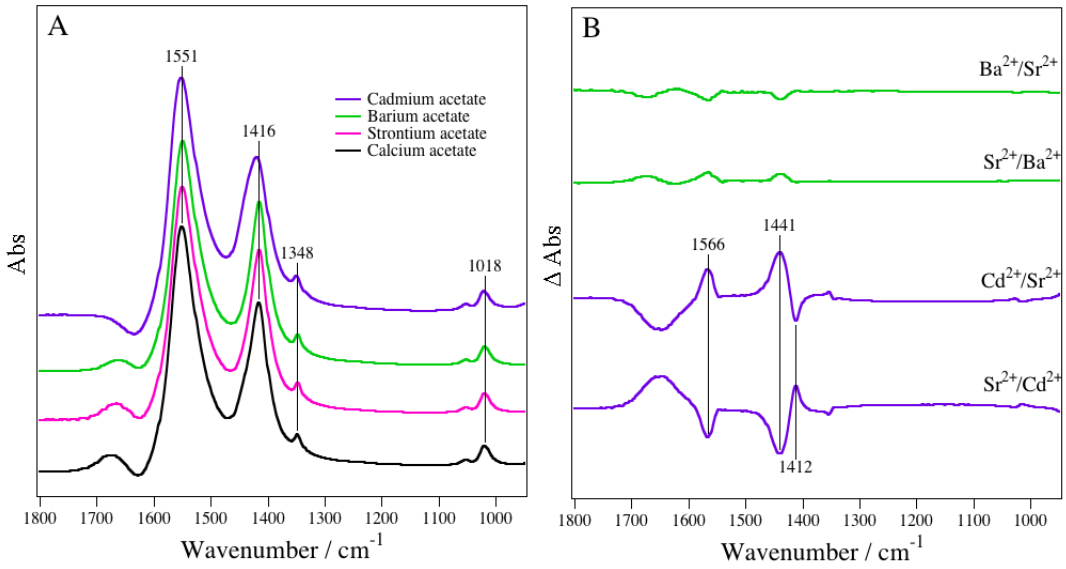

Figure 2-7. (A) ATR-FTIR absorption spectra of calcium acetate (black), strontium acetate (magenta), barium acetate (green), and cadmium acetate (purple) in aqueous solutions. (B) ATR-FTIR difference spectra between Ba^{2+}- and Sr^{2+}-spectra (green) or between Cd^{2+}- and Sr^{2+}-spectra (purple) after the normalization with respect to the peak intensity at 1018 cm^{-1}.

Figure 2-8. Amino acid sequences of the LH1 α- and β-polypeptides from purple sulfur bacteria [43, 79]. The amino acid ligands for Ca^{2+} identified in the new crystallographic structure [80] are indicated with red. The numbers represent the relative position of each residue to the conserved His bound to BChl-*a*.

Figure 2-9 shows ATR-FTIR absorption spectra of unlabeled and ^{15}N-labeled LH1-RC complexes from *Tch. tepidum*. The FTIR spectrum of unlabeled LH1-RC complex (black) exhibited prominent amide I and amide II bands at 1653 and 1545 cm^{-1}, respectively. Upon uniform ^{15}N-labeling of the LH1-RC complexes (magenta), the amide I band was slightly downshifted by ~2 cm^{-1}, due to a small coupling with the NH bending vibration, while the amide II band showed significant downshift by 14 cm^{-1} since the latter band is predominantly ascribed to the NH bending and CN stretching vibrations. These isotopic shifts were similar to those reported for PSII from isotope-labeled cyanobacteria [81, 82], strongly indicating that nitrogen atoms in the LH1-RC proteins are biosynthetically replaced with ^{15}N atoms. These results demonstrate that nitrogen atoms in the LH1-RC proteins are biosynthetically replaced with ^{15}N atoms.

Figure 2-10 shows ATR-FTIR difference spectra of ^{15}N-labeled LH1-RC complexes from *Tch. tepidum* upon the metal-exchanges. Although most of spectral features were similar with the corresponding difference spectra of unlabeled LH1-RC complexes (black), significant differences were evident as clearly seen in the $^{14}N/^{15}N$ double difference spectrum obtained by subtracting the unlabeled spectrum from the ^{15}N-labeled spectrum after the normalization with respect to the differential band at 891/883 cm^{-1} (Figure 2-11). Most prominent $^{15}N/^{14}N$ isotopic bands appeared in the 1600–1500 cm^{-1} region along with several mid-to-low intensity bands. The isotopic signals detected for the exchange from Ca^{2+} to Sr^{2+}, Ba^{2+} or Cd^{2+} were observed in the corresponding reversed spectrum from Sr^{2+}, Ba^{2+} or Cd^{2+} to Ca^{2+}, indicating that the $^{15}N/^{14}N$ isotopic bands are originating from the reversible structural changes of polypeptide backbones and amino acid side chains containing nitrogen atoms in the vicinity of the metal-binding site at the C-terminal side of the *Tch. tepidum* LH1

proteins. In addition, the $^{15}N/^{14}N$ isotopic bands for the Sr^{2+}-substitution were largely similar with those for the Ba^{2+}-substitution but were distinctively different with those for the Cd^{2+}-substitution in the 1700 – 1500 cm^{-1} region. This indicates that structural changes of the amide modes containing and/or coupled to ^{15}N were uniquely modified upon the Cd^{2+}-substitution.

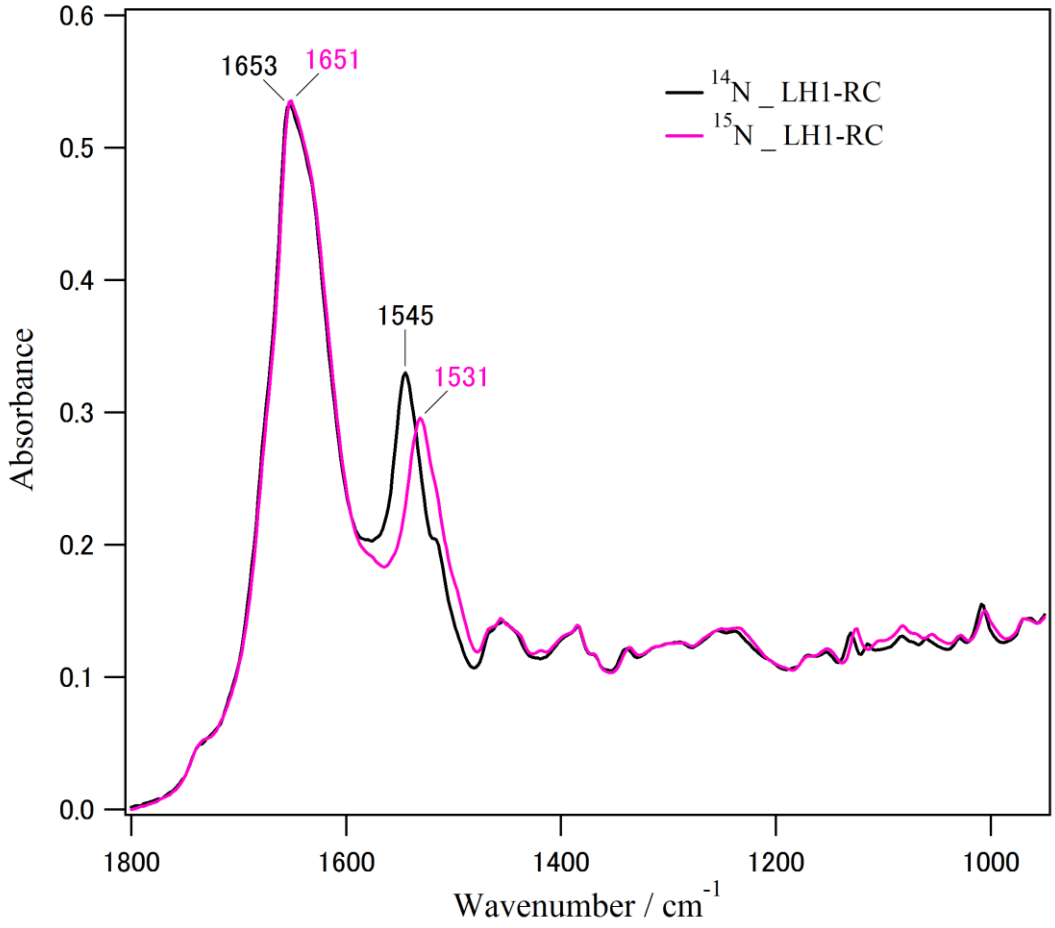

Figure 2-9. Absorption spectra of unlabeled (black) and ^{15}N-labeled (magenta) LH1-RC complexes from *Tch. tepidum*.

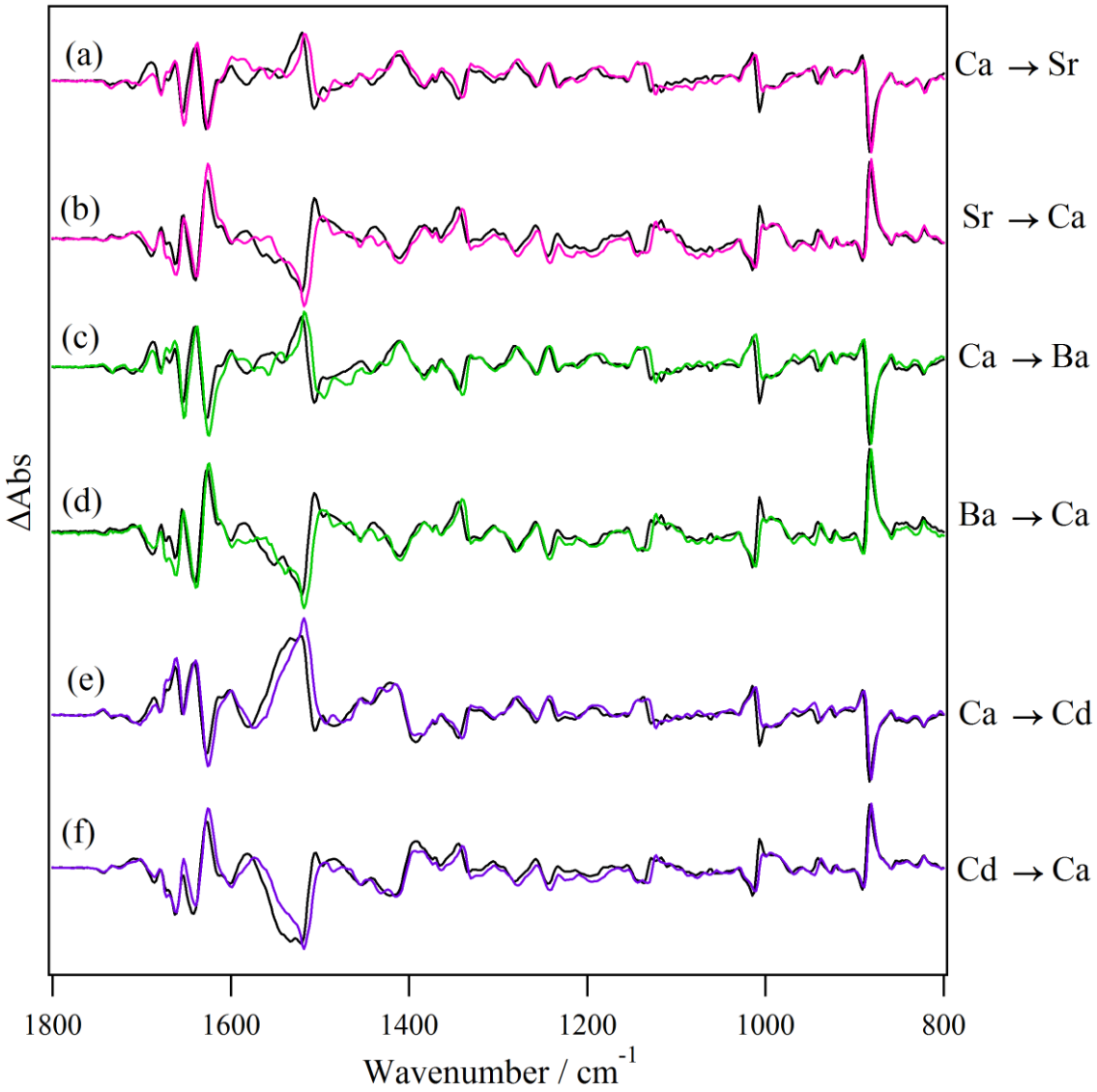

Figure 2-10. ATR-FTIR difference spectra of ^{15}N-labeled LH1-RC complexes from *Tch. tepidum* upon Sr^{2+}/Ca^{2+} (a, magenta), Ca^{2+}/Sr^{2+} (b, magenta), Ba^{2+}/Ca^{2+} (c, green), Ca^{2+}/Ba^{2+} (d, green), Cd^{2+}/Ca^{2+} (e, purple), and Ca^{2+}/Cd^{2+} (f, purple) exchanges. The corresponding difference spectra of unlabeled LH1-RC complexes were presented for comparison (a-f, black).

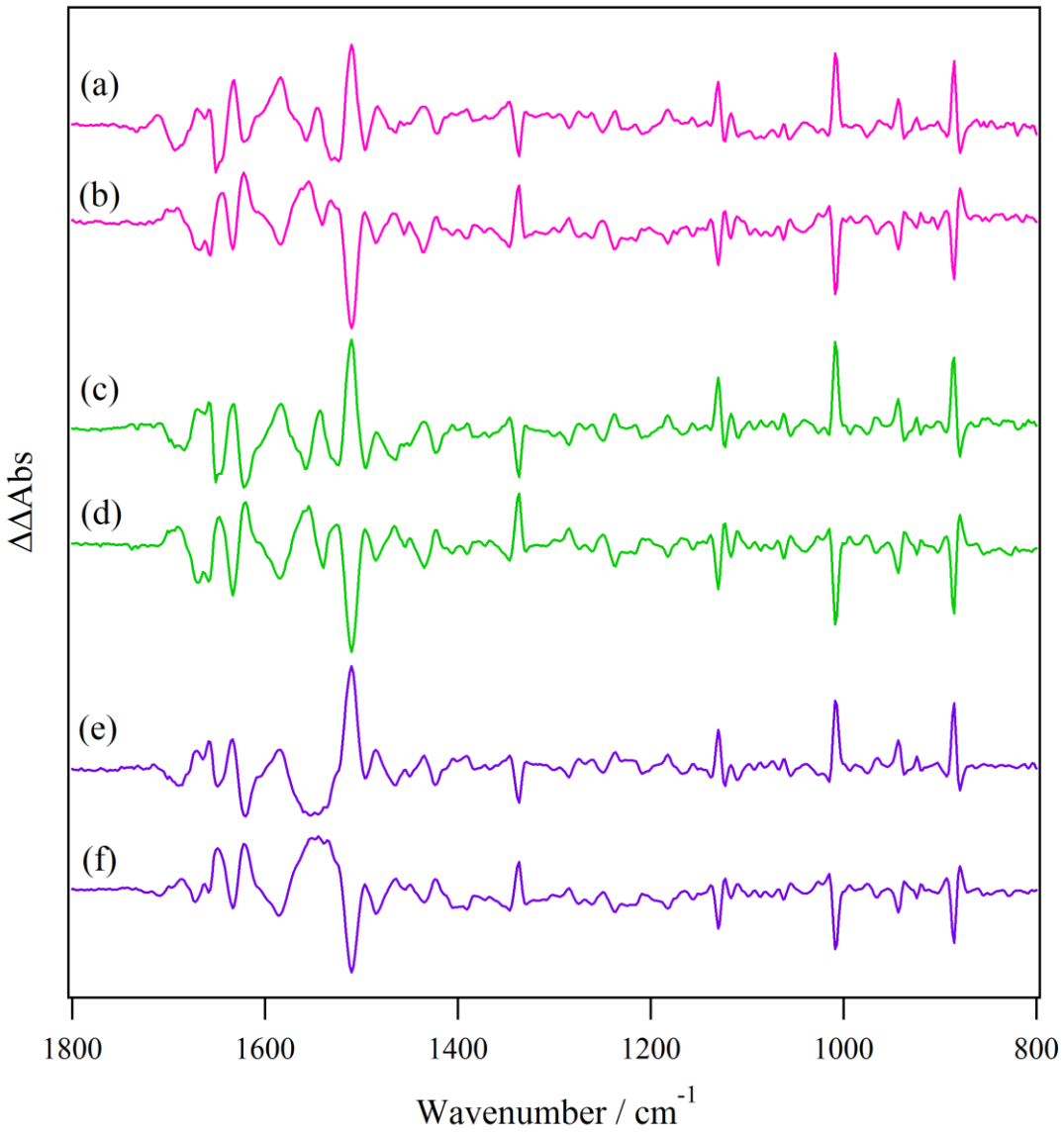

Figure 2-11. $^{15}N/^{14}N$ double difference spectra obtained by subtracting the unlabeled spectrum from the ^{15}N-labeled spectrum upon Sr^{2+}/Ca^{2+} (a, magenta), Ca^{2+}/Sr^{2+} (b, magenta), Ba^{2+}/Ca^{2+} (c, green), Ca^{2+}/Ba^{2+} (d, green), Cd^{2+}/Ca^{2+} (e, purple), and Ca^{2+}/Cd^{2+} (f, purple) exchanges after the normalization with respect to the differential band at 891/883 cm^{-1}.

Figure 2-12 shows ATR-FTIR absorption spectra of unlabeled and ^{13}C-labeled LH1-RC complexes from *Tch. tepidum*. The FTIR spectrum of unlabeled LH1-RC complex (black) exhibited prominent amide I and amide II bands at 1653 and 1545 cm^{-1}, respectively. Upon uniform ^{13}C-labeling of the LH1-RC complexes (red), the amide I band showed a significant downshift by 37 cm^{-1}, while the amide II band was moderately downshifted by 12 cm^{-1}. These isotopic shifts were similar to those reported for PSII from isotope-labeled cyanobacteria [81, 82], strongly indicating that carbon atoms in the LH1-RC proteins are biosynthetically replaced with ^{13}C atoms.

Figure 2-13 shows ATR-FTIR difference spectra of ^{13}C-labeled LH1-RC complexes from *Tch. tepidum* upon the metal-exchanges. Most of the bands were significantly downshifted upon the ^{13}C-labeling as compared with the corresponding difference spectra of unlabeled LH1-RC complexes (black). The differences were more clearly seen in the $^{13}C/^{12}C$ double difference spectrum obtained by subtracting the unlabeled spectrum from the ^{13}C-labeled spectrum after the normalization with respect to the differential band at 891/883 cm^{-1} (Figure 2-14). Intensive $^{13}C/^{12}C$ isotopic bands appeared in the 1700 – 1500 cm^{-1} and 900 – 850 cm^{-1} regions along with several mid-to-low intensity bands in the 1500 – 900 cm^{-1} region. The isotopic signals detected for the exchange from Ca^{2+} to Sr^{2+}, Ba^{2+} or Cd^{2+} were observed in the corresponding reversed spectrum from Sr^{2+}, Ba^{2+} or Cd^{2+} to Ca^{2+}, indicating that the $^{13}C/^{12}C$ isotopic bands are originating from the reversible structural changes of polypeptide backbones and amino acid side chains containing carbon atoms in the vicinity of the metal-binding site at the C-terminal side of the *Tch. tepidum* LH1 proteins. In contrast to the ^{15}N-isotope effects, the $^{13}C/^{12}C$ isotopic bands were modified depending on the cation species; effects by the Sr^{2+}-substitution were slightly different from those by the Ba^{2+}-substitution in the 1700 –1500 cm^{-1} region,

and largely by the Cd^{2+}-substitution in the 1700 –1350 cm^{-1} region. These results suggest that the binding modes of several residues and/or polypeptide main and side chains comprising the metal binding site are differently affected depending on the metal cations.

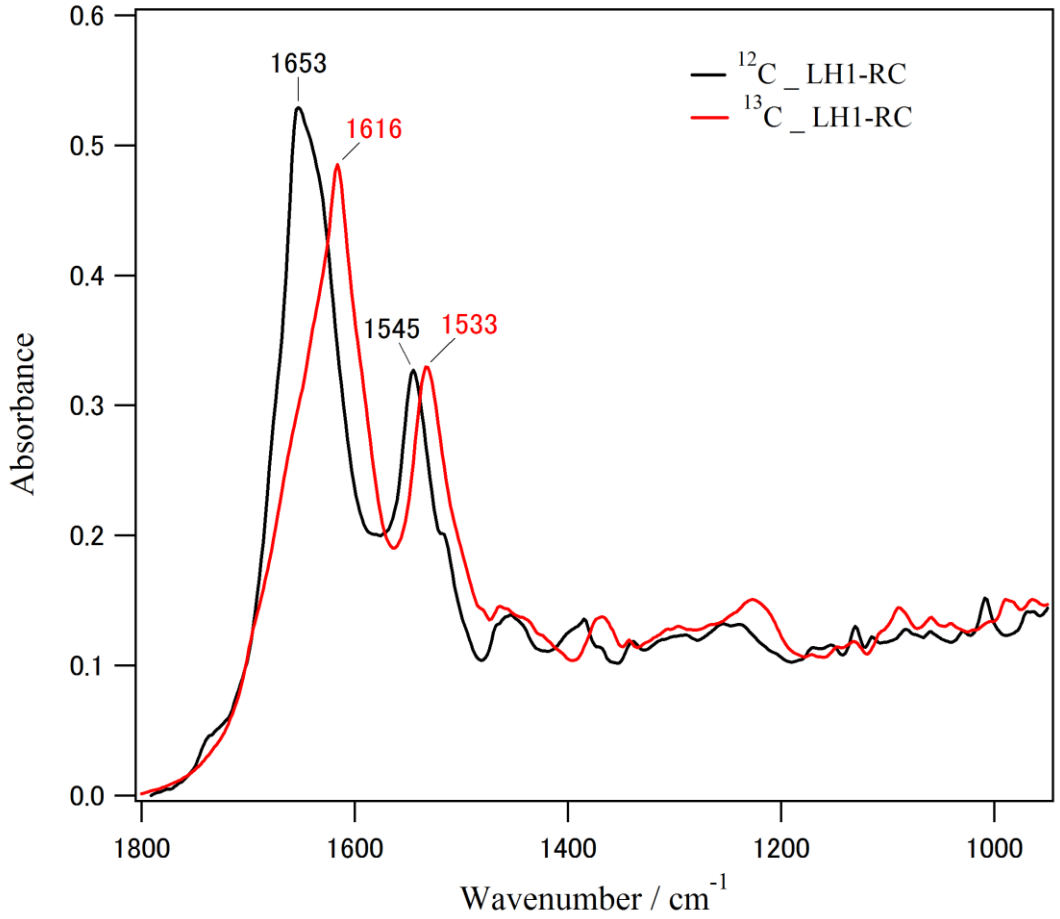

Figure 2-12. Absorption spectra of unlabeled (black) and ^{13}C-labeled (red) LH1-RC complexes from *Tch. tepidum*.

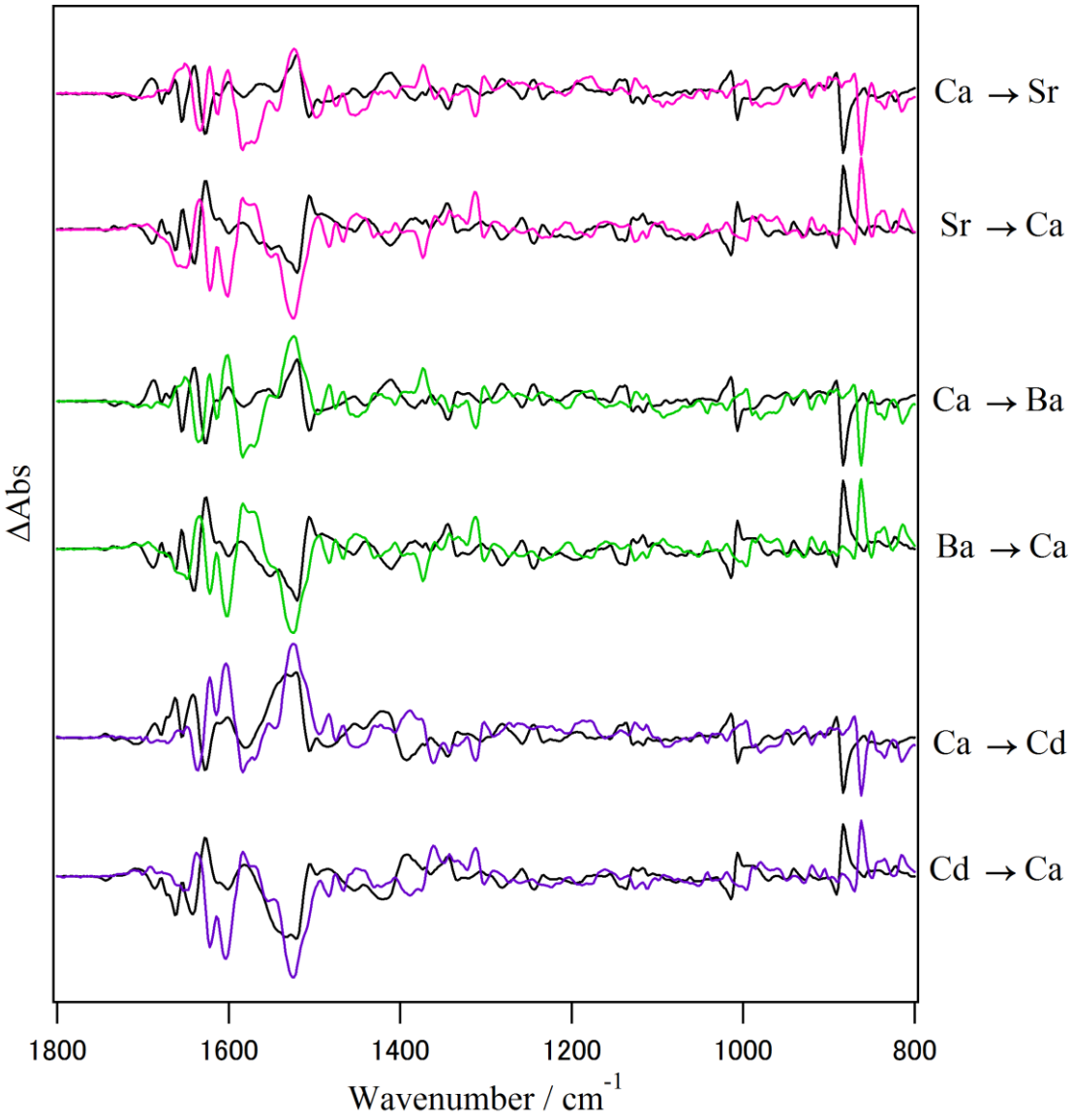

Figure 2-13. ATR-FTIR difference spectra of ^{13}C-labeled LH1-RC complexes from *Tch. tepidum* upon Sr^{2+}/Ca^{2+} (a, magenta), Ca^{2+}/Sr^{2+} (b, magenta), Ba^{2+}/Ca^{2+} (c, green), Ca^{2+}/Ba^{2+} (d, green), Cd^{2+}/Ca^{2+} (e, purple), and Ca^{2+}/Cd^{2+} (f, purple) exchanges. The corresponding difference spectra of unlabeled LH1-RC complexes were presented for comparison (a-f, black).

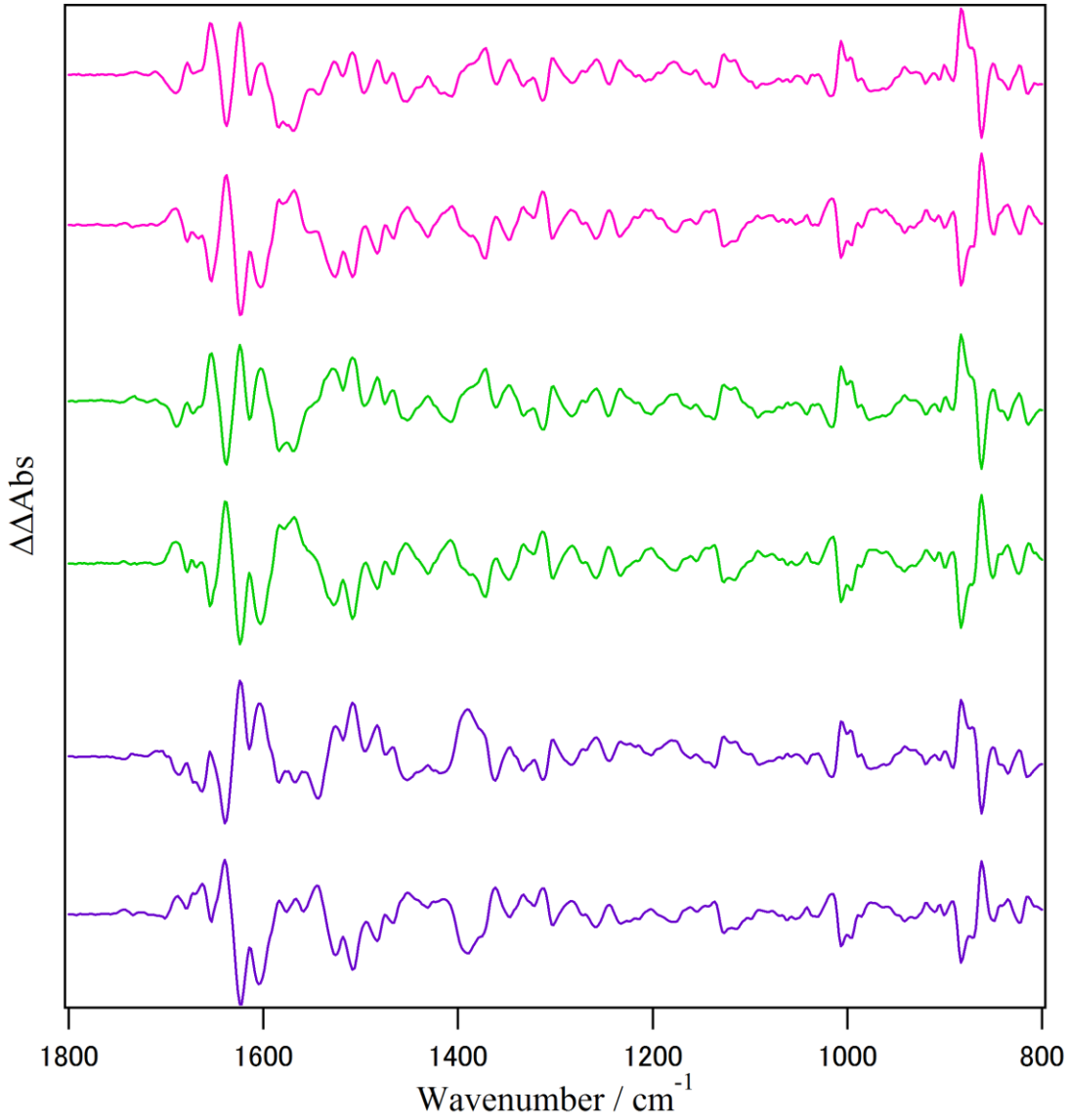

Figure 2-14. $^{13}C/^{12}C$ double difference spectra obtained by subtracting the unlabeled spectrum from the ^{13}C-labeled spectrum upon Sr^{2+}/Ca^{2+} (a, magenta), Ca^{2+}/Sr^{2+} (b, magenta), Ba^{2+}/Ca^{2+} (c, green), Ca^{2+}/Ba^{2+} (d, green), Cd^{2+}/Ca^{2+} (e, purple), and Ca^{2+}/Cd^{2+} (f, purple) exchanges after the normalization with respect to the differential band at 891/883 cm^{-1}.

Figure 2-15 shows absorption spectra of unlabeled (black) and ^{2}H-labeled (blue) LH1-RC complexes from *Tch. tepidum*. The intensities of typical amide I and II bands at ~1653 cm^{-1} and ~1545 cm^{-1}, respectively, were reduced and new bands appeared at ~1454 cm^{-1} for amide II′ mode (νCN and δND) of deuterated polypeptide backbones and at ~1206 cm^{-1} for the DOD bending mode. These spectral changes are largely compatible with that reported previously for the PSII complex from *Thermosynechococcus elongatus* [83], indicating that most of hydrogen atoms in the LH1-RC complexes are replaced with deuterium.

Figure 2-16 shows ATR-FTIR difference spectra of ^{2}H-labeled LH1-RC complexes from *Tch. tepidum* upon the metal-exchanges. The bands in the 1700–1500 cm^{-1} and 1300–1200 cm^{-1} regions were significantly affected by the ^{2}H-labeling as compared with the corresponding difference spectra of unlabeled LH1-RC complexes (black). However, several bands in the 1450–1300 cm^{-1} and 1150–850 cm^{-1} regions were little changed upon the deuteration. The differences were more clearly seen in the ^{2}H/^{1}H double difference spectrum obtained by subtracting the unlabeled spectrum from the ^{2}H-labeled spectrum after the normalization with respect to the differential band at 891/883 cm^{-1} (Figure 2-17). The prominent ^{2}H/^{1}H double difference bands were apparent in the 1700–1500 cm^{-1} region which potentially includes amide I and II modes, νC=O of Asn or Gln, $\nu_{as}CN_3H_5^+$ of Arg, $\delta_{as}NH_3^+$ and $\delta_{s}NH_3^+$ of Lys, δNH_2 of Asn and Gln, several vibrational modes of Trp, Tyr, and His residues [73]. On the basis of the isotopic shifts by ^{15}N-, ^{13}C-, and ^{2}H-labelings, the difference bands detected upon Sr^{2+}-substitution are tentative assigned and summarized in Table 2-1.

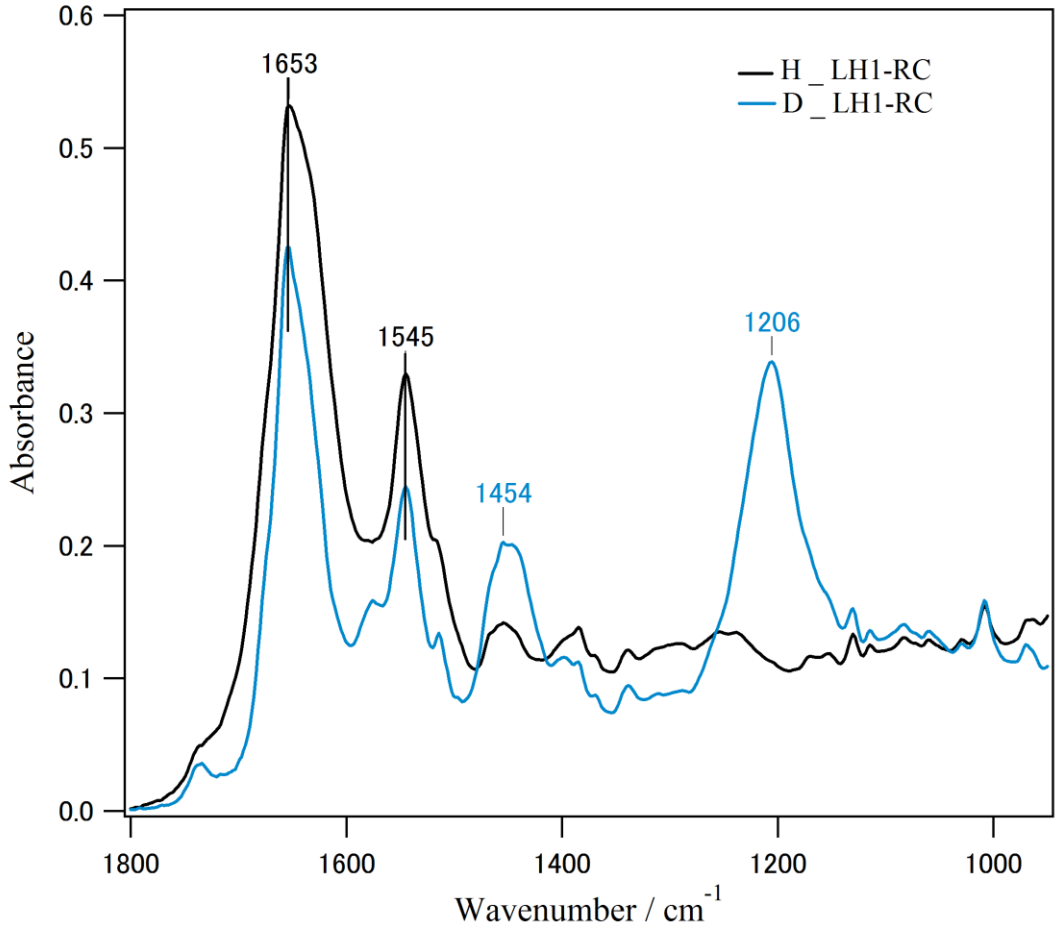

Figure 2-15. Absorption spectra of unlabeled (black) and ^{2}H-labeled (blue) LH1-RC complexes from *Tch. tepidum*.

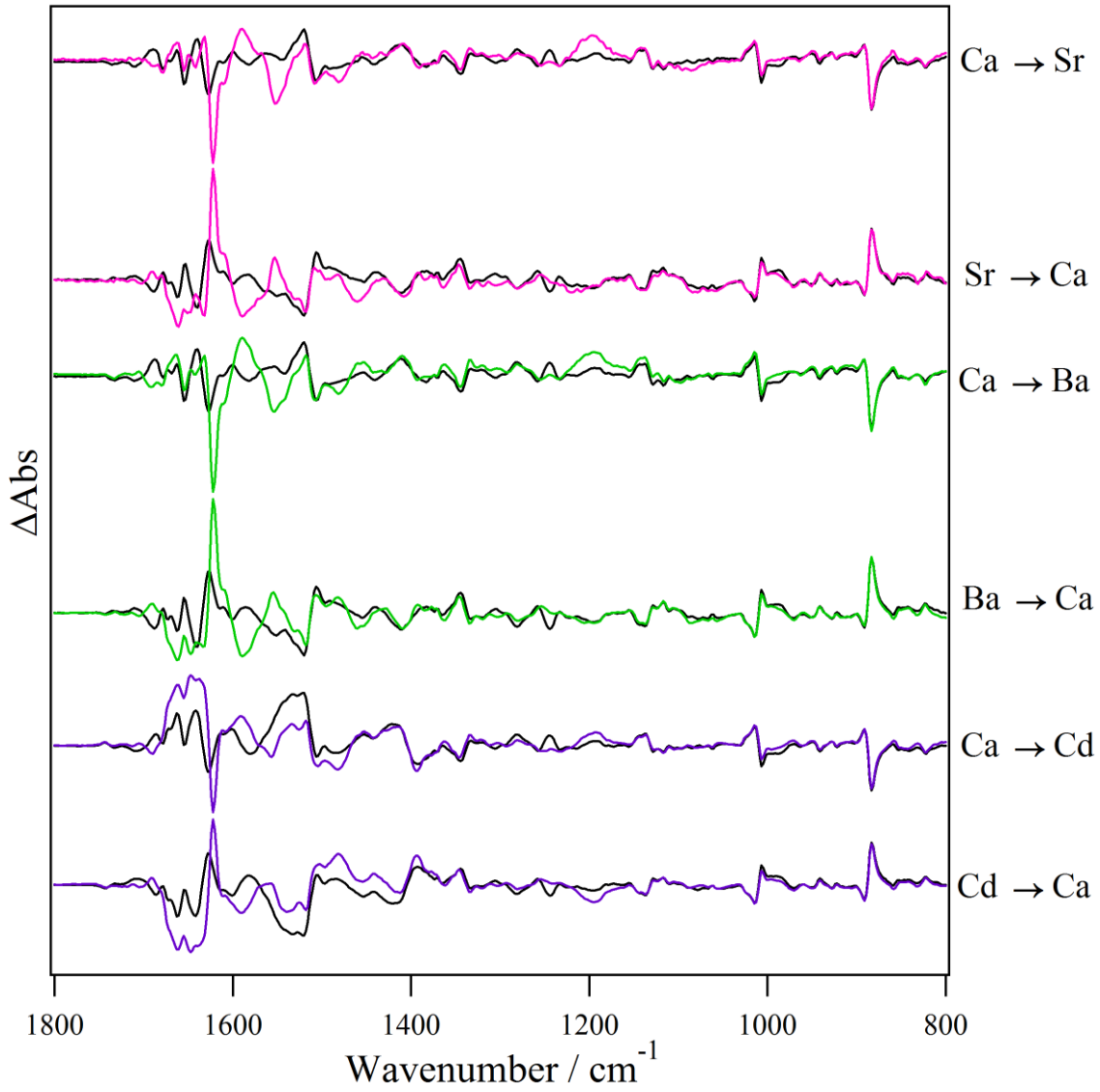

Figure 2-16. ATR-FTIR difference spectra of ^{2}H-labeled LH1-RC complexes from *Tch. tepidum* upon Sr^{2+}/Ca^{2+} (a, magenta), Ca^{2+}/Sr^{2+} (b, magenta), Ba^{2+}/Ca^{2+} (c, green), Ca^{2+}/Ba^{2+} (d, green), Cd^{2+}/Ca^{2+} (e, purple), and Ca^{2+}/Cd^{2+} (f, purple) exchanges. The corresponding difference spectra of unlabeled LH1-RC complexes were presented for comparison (a-f, black).

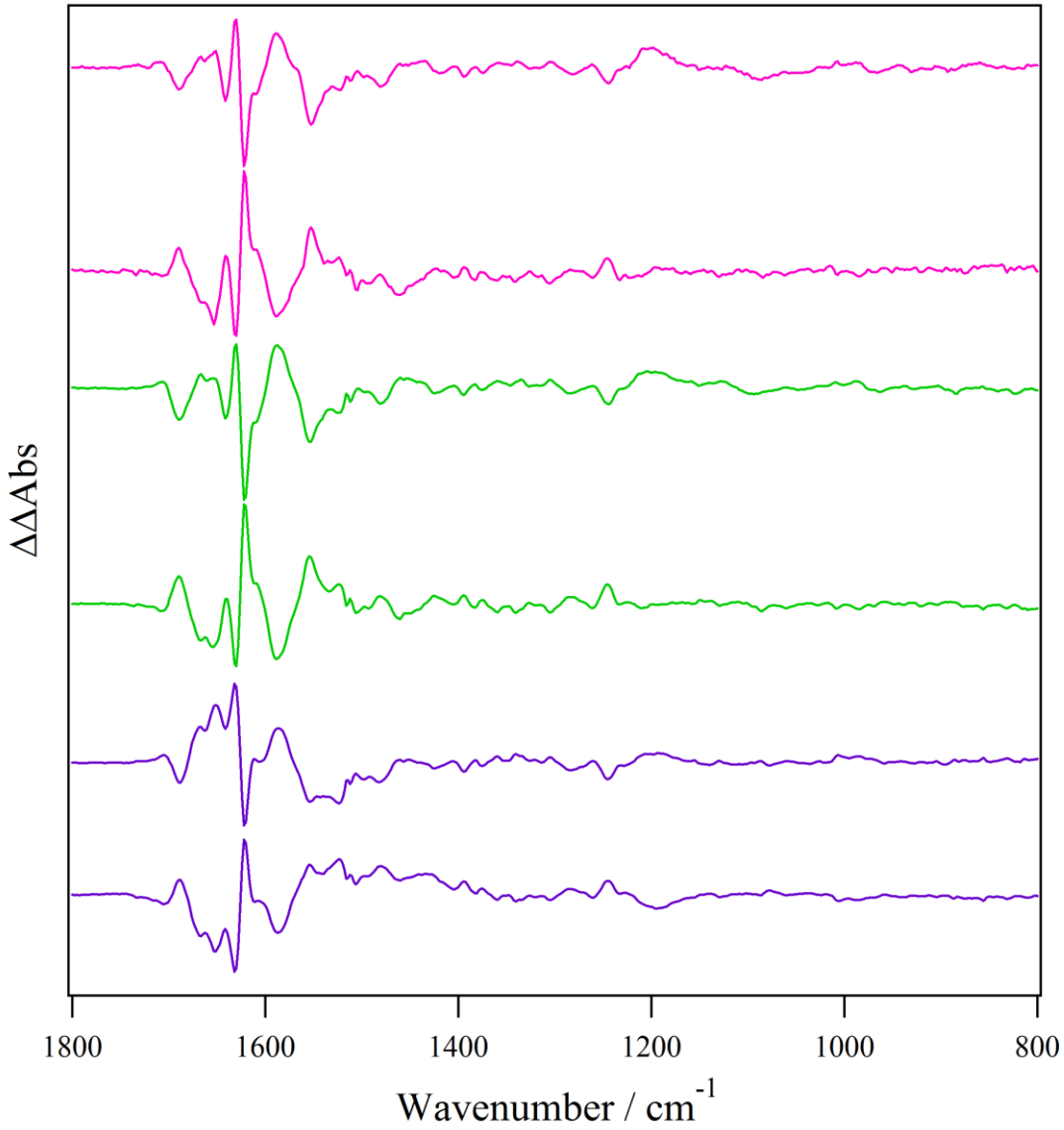

Figure 2-17. $^{2}H/^{1}H$ double difference spectra obtained by subtracting the unlabeled spectrum from the ^{13}C-labeled spectrum upon Sr^{2+}/Ca^{2+} (a, magenta), Ca^{2+}/Sr^{2+} (b, magenta), Ba^{2+}/Ca^{2+} (c, green), Ca^{2+}/Ba^{2+} (d, green), Cd^{2+}/Ca^{2+} (e, purple), and Ca^{2+}/Cd^{2+} (f, purple) exchanges after the normalization with respect to the differential band at 891/883 cm^{-1}.

In the present study, I selected metal cations (Sr^{2+}, Ba^{2+}, and Cd^{2+}) as useful metal probes in the *Tch. tepidum* LH1-RC complex because of the following reasons: (1) Sr^{2+} is the sole metal cation which is biosynthetically replaceable with Ca^{2+} [41], (2) spectroscopic and thermodynamic effects by Ba^{2+}-substitution are very similar with those by Sr^{2+}-substitution [12, 40], and (3) Cd^{2+} has the divalent cation with almost identical ionic radius with Ca^{2+} [50]. However, the most appropriate metal cation for monitoring the Ca^{2+}-binding site is $^{44}Ca^{2+}$, the stable isotope of Ca^{2+}, which induces a minimum perturbation in the binding site and is possible to detect selectively the structural changes within the first coordination sphere. Therefore, I examined the effects of $^{44}Ca^{2+}$-substitution on the ATR-FTIR difference spectra of the LH1-RC complexes from *Tch. tepidum* (spectra a in Figure 2-18). Several bands due to the changes of the background appeared in the $^{44}Ca^{2+}/^{40}Ca^{2+}$ ($^{40}Ca^{2+}/^{44}Ca^{2+}$) difference spectra. However, no significant $^{44}Ca^{2+}/^{40}Ca^{2+}$ bands were detected in comparison with the difference bands detected upon the Sr^{2+}-substitution (spectra b). A possible explanation is that each interaction between Ca^{2+} and the ligand is not strong and the increased mass of Ca^{2+} little affect on the vibrational modes of polypeptide main chain and amino acid side chains appearing in the present mid-frequency region. If this is the case, some Ca^{2+}-ligand modes appearing in the low-frequency region (< 800 cm^{-1}) may exhibit significant isotope shifts upon the $^{44}Ca^{2+}$-substitution.

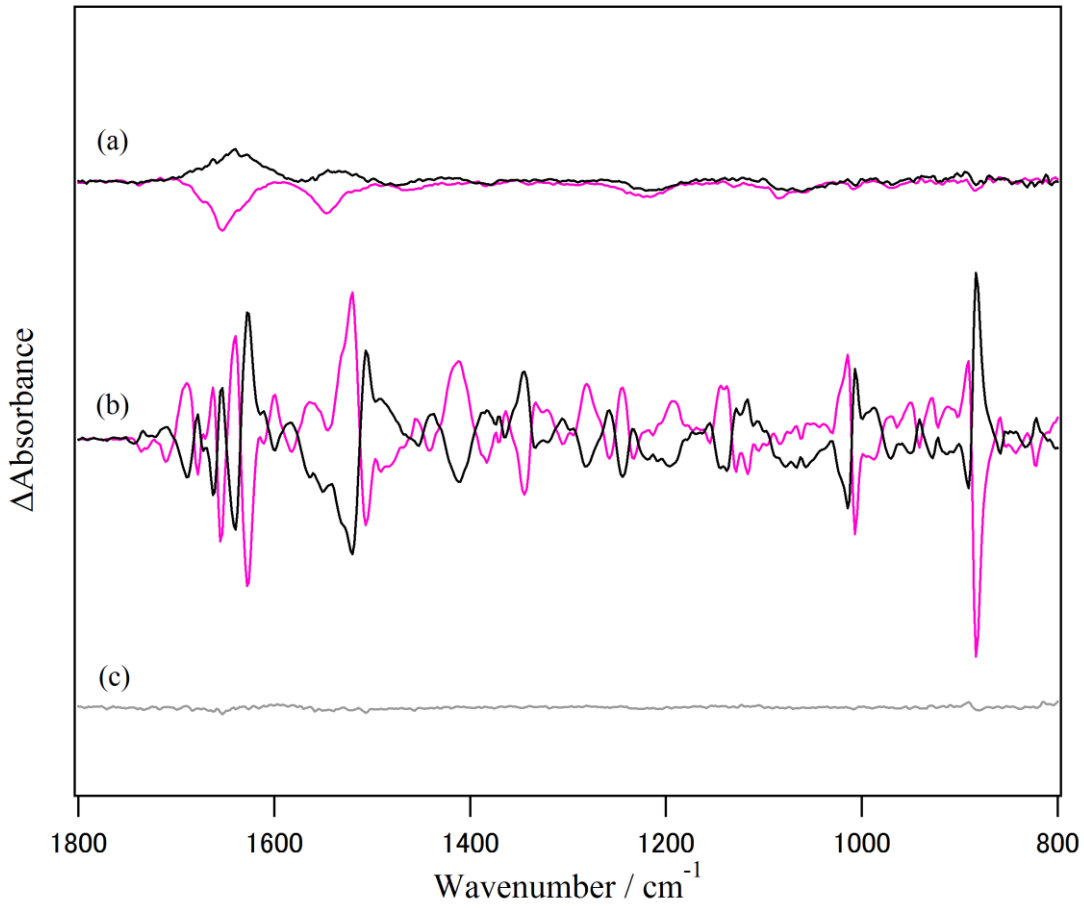

Figure 2-18. ATR-FTIR difference spectra of the LH1-RC complexes from *Tch. tepidum* induced by switching from Ca^{2+}-buffer to $^{44}Ca^{2+}$-buffer ($^{44}Ca^{2+}/^{40}Ca^{2+}$ difference spectrum, a, magenta) and the following reversed spectrum ($^{40}Ca^{2+}/^{44}Ca^{2+}$ difference spectrum, a, black), and difference spectrum(b). The difference spectra of the LH1-RC complex induced by the Sr^{2+}-substitution (b) and the noise level (c) are presented for comparison.

Table 2-1. ATR-FTIR difference bands of the *Tch. tepidum* LH1-RC complexes upon Sr^{2+}-substitution and tentative assignments of each band based on the isotopic shifts upon uniform ^{15}N- ,^{13}C- and ^{2}H-labelings.

Unlabeled	^{15}N-labeled ($\Delta^{15}N$)	^{13}C-labeled ($\Delta^{13}C$)	D-labeled (ΔD)	Tentative assignment
1736	1734 (-2)	1695(-41)	1690(-46)	BChl νC=O
1690	1688(-2)	1651(-39)	1663(-27)	Asn νC=O, Amide I turn (Trp),random coil
1663	1663(0)	1622(-41)	1663(0)/1649(-14)	Amide I α-helix, turn,random coil
1655	1653(-2)	1613(-42)	1655(0)/1641(-14)	Amide I α-helix, turn, random coil
1640	1638(-2)	1601(-39)	1632(-8)	Amide I α-helix
1628	1626(-2)	1584(-44)	1622(-6)	ν_{as} COO^-
1599	1599(0)	1553(-46)	1589(-10)	Tyr νC=C
1582	1557(-25)	1545(-37)	1481(-101)	Amide II
1564	1545(-9)	1524(-40)	1454(-110)	Amide II
1520	1518(-2)	1483(-37)	1520(0)	ν_{as} COO^-, Tyr νC=C
1506	1495(-11)	1476(-30)	1508(+2)	Amide II, Trp νCN
1412	1410(-2)	1373(-39)	1410(-2)	ν_s COO^-
1383	1383(0)	1360(-23)	1391(+8)	ν_s COO^-
1373	1373(0)	1350(-23)	1373(0)	ν_s COO^-
1364	1364(0)	1323(-41)	1364(0)	ν_s COO^-
1344	1341(-3)	1317(-27)	1344(0)	ν_s COO^-
1333	1331(-2)	1302(-23)	1335(+2)	ν_s COO^-
1281	1279(-2)	1260(-12)		ν_s COO^- ν_s COO^-, Trp, Try
1258	1256(-2)	1246(-10)		Tyr δCOH
1244	1242(-2)	1234(-10)		Tyr δCOH
1233	1231(-2)	1219(-14)		Tyr δCOH
1144	1144(0)	1136(-8)	1144(0)	νC-O
1138	1134(-4)	1123(-15)	1138(0)	νCN
1128	1123(-5)	1094(-34)	1128(0)	His νCN
1117	1105(-12)	1082(-35)	1117(0)	His νCN
1015	1013(-2)	997(-18)	1015(0)	ν_{as} CNC
1007	1003(-4)	990(-17)	1007(0)	ν_{as} CNC
891	891(0)	870 (-21)	891(0)	ν_s CNC
883	881(-2)	862 (-21)	883(0)	ν_s CNC
858	860(+2)	851 (-9)	858(0)	ν_s CNC

2.3.4 Tentative Assignments of the Perfusion-induced ATR-FTIR Difference Bands

Based on the primary sequence [43] and a topological analysis [70], it was proposed that the Ca^{2+}-binding site is comprised of several acidic residues located at the C-terminal region of the LH1 $\alpha\beta$-polypeptides [12, 70]. Several spectroscopic analyses indicated that the metal-depletion/substitution induced few changes in the secondary and tertiary structures of the LH1-RC complex [12, 74, 75]. However, the present ATR-FTIR study detected clear metal-sensitive difference bands in the 1800–800 cm^{-1} region which includes characteristic vibrational modes of polypeptide main chains and amino acid side chains in the LH1-RC complex. These results indicate that small but significant conformational modifications upon the metal exchange occur in the structures that are directly and/or indirectly interacting with Ca^{2+} in the LH1 C-terminal region.

It is noteworthy here that very recently a new crystallographic structure of the *Tch*. *tepidum* LH1-RC complex has been presented [80]. As predicted in the previous studies [12, 70, 74, 75], the LH1 complex is 16-mer of the $\alpha\beta$-subunit, each of which has a Ca^{2+}-binding site comprised of α-Trp_{+10}, α-Asp_{+13}, α-Asn_{+14}, and β-Leu_{+10} locating at the C-terminal region of the LH1 $\alpha\beta$-subunit (Figure 2-8). The carboxylate side chain of α-Asp_{+13} and the C-terminal carboxylate of β-Leu_{+10} coordinate with Ca^{2+} in unidentate and bidentate manners, respectively. Generally, metal-carboxylate complexes exhibit asymmetric (ν_{as}) COO^- stretching mode at 1675−1515 cm^{-1} and symmetric (ν_s) COO^- stretching mode at 1495−1260 cm^{-1} [84], and the metal-carboxylate ligation structures are empirically relevant to the value of $\Delta\nu$ ($=\nu_{as}-\nu_s$); $\Delta\nu$= ~164 cm^{-1} for ionic form, $\Delta\nu >>$ ~164 cm^{-1} for unidentate form, $\Delta\nu =$ ~164 cm^{-1} (but greater than $\Delta\nu$ for bidentate) for bridging form, and $\Delta\nu <$ ~164 cm^{-1}

for bidentate form [85, 86]. Unfortunately, this is not applicable to the present results since the intensive bands in the amide I and II regions are largely overlapping with the asymmetric COO^- bands, and therefore, the close inspection of the ν_{as} bands is hard to achieve dispense with isotope-edited analyses. In contrast, the symmetric COO^- stretching bands (1495−1260 cm^{-1}) can be analyzed more clearly since the intensive amide I and II bands are absent in this region, and CH_2 scissoring (1480–1440 cm^{-1}) and CH_3 deformation modes (1465–1440 cm^{-1} and 1390–1370 cm^{-1}) are less sensitive to faint changes in the molecular environment. Thus, the bands at 1443/1383/1371/1306/1294 cm^{-1} and 1456/1410/1364/1333/1321 cm^{-1} in the Sr^{2+}/Ca^{2+} (Ca^{2+}/Sr^{2+}) difference spectra (Figure 2-3) are possible candidates for the symmetric COO^- stretching bands of α-Asp_{+13} and β-Leu_{+10} ligating Ca^{2+} and Sr^{2+}, respectively. In addition, the symmetric COO^- stretching bands of carboxylates in a unidentate ligation tend to appear at lower frequencies than that in a bidentate ligation [86]. If this is the case, the ν_s bands of α-Asp_{+13} and β-Leu_{+10} correspond to the lower and higher frequencies, respectively, of the putative bands. However, I can not exclude the possibility that the 1495−1260 cm^{-1} region includes contribution from other vibrational modes; the symmetric COO^- stretching of another Asp residue indirectly coupled with the Ca^{2+}-binding site (no Glu residue is located at the C-terminal side), the C-N stretching of -$CONH_2$ from Asn and Gln (1420−1400 cm^{-1}), and the O-H deformation of Tyr, Thr, and Ser (1440−1260 cm^{-1}) [84].

Several intensive differential bands (1690/1678/1663/1655/1639/1628/1599 cm^{-1}) in the 1700–1600 cm^{-1} may be assigned to the amide I mode of the main chains (1695–1623 cm^{-1}). It is known that the frequencies of the amide I bands reflect the secondary structures; 1657–1648 cm^{-1} for α-helix, 1695–1674 cm^{-1} and 1641–1623 cm^{-1} for β-sheet, 1686–1662 cm^{-1} for turns, and 1670–1660 cm^{-1} for random coil [73,

84]. However, the contribution of β-sheet structures are excluded since the LH1 $\alpha\beta$-subunits are predominantly comprised of transmembrane α-helices as well as turns and random coil structures at the C- and N-terminal sides [80]. Therefore, the bands at 1695–1674 cm^{-1} and 1641–1623 cm^{-1} can be assigned to other bands including the C=O stretching of Asn (1678–1677 cm^{-1}, or up to 1704 cm^{-1} in proteins) and Gln (1687–1668 cm^{-1}), the asymmetric and symmetric $CN_3H_5^+$ stretching of Arg (1695–1652 and 1663–1614 cm^{-1}, respectively), the NH_3^+ deformation of Lys (1629–1626 cm^{-1}), and the NH_2 bending of Asn (1622–1612 cm^{-1}) [73, 87, 88]. In particular, contribution of α-Asn_{+14} to the metal-sensitive FTIR bands at 1677–1678 cm^{-1} and 1612–1622 cm^{-1} is likely to be involved since its carbonyl side chain serves as a direct ligand for Ca^{2+} [80].

In addition, the carbonyl main chain of α-Trp_{+10} exists in the first coordination sphere of the Ca^{2+}-binding site and is involved in the turn structure at the C-terminal region of the LH1 *a*-polypeptide [80]. Therefore, the 1686–1662 cm^{-1} bands are putatively ascribed to the main chain of α-Trp_{+10}. The α-Trp_{+10} and β-Trp_{+9} residues are highly conserved among purple bacteria at the C-terminal region of LH1 polypeptides [79], and proposed as hydrogen-bonding partners of the C3-acetyl C=O groups of BChl-*a* molecules for tuning the LH Q_y transition energy through the hydrogen-bonds [89, 90]. A previous Raman study strongly indicated that the hydrogen-bonding interactions between BChl-*a* and LH1 α-Trp_{+10}/β-Trp_{+9} are modulated by the metal cations in the *Tch. tepidum* LH1-RC complex [42]. Based on these results, it is possible that conformational changes of α-Trp_{+10} residues and/or BChl molecules (1760–1680 cm^{-1}) [91] are also involved in the metal-sensitive ATR-FTIR signals.

In the 1600–1500 cm^{-1} region, possible candidates for the intensive bands at

1531(shoulder)/1520/1506 cm^{-1} and mid-to-low intensity bands at 1599/1582/1564 cm^{-1} are the amide II modes of the polypeptide main chain (1577–1507 cm^{-1}) [81, 82, 84], the asymmetric stretching modes of COO^- from α-Asp_{+13} side chain and C-terminal carboxylate of β-Leu_{+10} (1675−1515 cm^{-1}, depending on the ligation structure) [85, 86], and/or the CC stretching of Tyr (1602–1594 cm^{-1} and 1518–1516 cm^{-1}) [73]. In addition, other bands for the symmetric deformation of NH_3^+ from Lys (1527–1526 cm^{-1}), and the CN stretching and CH/NH bending of Trp (1509 cm^{-1}) are possible to be involved in this region [73].

2.4 Conclusion

Thermochromatium (*Tch*.) *tepidum* is a purple sulfur photosynthetic bacterium which can grow at 58˚C, the highest temperature among purple bacteria, and exhibits an unusually red-shifted Q_y transition of the light-harvesting 1 reaction center (LH1-RC) complex at 915 nm (B915). These unique properties are closely related with an inorganic cofactor, Ca^{2+}, of which the putative binding site is proposed to be residing at the C-terminal region of the LH1 α-subunits. However, the molecular mechanism how this organism acquired the enhanced thermal stability and unusual spectroscopic property by utilizing Ca^{2+} is still an open question.

In the present study, I detected for the first time metal-sensitive fine structural changes of protein backbones and amino acid side chains by means of perfusion-induced ATR–FTIR spectroscopy, and provide structural indications responsible for the enhanced thermal stability of the *Tch. tepidum* LH1-RC complex upon the binding of Ca^{2+}. The essential points of this study are as follows:

1. I constructed perfusion-induced ATR-FTIR measuring system and detected for the first time the structural changes of polypeptide backbones and amino acid side chains in the *Tch. tepidum* LH1-RC proteins upon the replacement of native Ca^{2+} with other metal cations (Sr^{2+}, Ba^{2+}, Cd^{2+}).

2. The metal-sensitive ATR-FTIR bands were tentatively assigned based on the isotope shifts upon uniform ^{15}N, ^{13}C, and ^{2}H-labelings.

3. The structural changes induced by the exchange between two metal cations were fully reversible and specific for the *Tch. tepidum* LH1-RC complex based on a comparative analysis using the mesophilic counterpart, *Allochromatium vinosum*.

4. The LH1 complex lacking the RC was first isolated and characterized in *Tch. tepidum*. The ATR-FTIR signals for the LH1 complex were almost identical with those of the LH1-RC complex. These and previous results strongly indicated that the metal-sensitive ATR-FTIR bands originate from polypeptide backbones and amino acid residues near the putative Ca^{2+}-binding site located at the C-terminal side of the *Tch. tepidum* LH1 $\alpha\beta$-polypeptides.

5. The structural modifications induced by the Ba^{2+}-substitution were basically identical with those by the Sr^{2+}-substitution. In contrast, the Cd^{2+}-substitution exhibited unique structural modifications, particularly in the amide I and II, and carboxylate modes, which may be responsible for the severely deteriorated thermal stability of the Cd^{2+}-substituted complex and are intimately related with the molecular mechanism for the enhanced thermal stability of *Tch. tepidum*.

Chapter 3 Structural and functional roles of calcium ions and extrinsic proteins in the oxygen-evolving complex of photosystem II

3.1 Introduction

Oxygenic phototrophs convert photon energy into chemical energy through a series of light-induced electron transfer reactions initiated with charge separation of chlorophyll special pairs located in the central part of photosystem I and II (PSI and PSII). The reducing power is transferred from PSII to PSI through cytochrome b_6f, and finally utilized for reduction of $NADP^+$ to assimilate CO_2. The oxidized equivalents accumulated on the PSII donor side are neutralized by substrate water molecules to release protons for driving ATP synthase and O_2 molecules as a by-product. This water oxidation takes place in the oxygen-evolving complex (OEC) of PSII [34, 92]. The OEC assembly is largely similar between cyanobacteria and higher plants, except for a critical difference in the composition of extrinsic proteins [26]. In cyanobacteria, PsbO, PsbV, and PsbU residing on the lumenal side of PSII play significant roles in the regulation and stabilization of the water oxidation machinery. Higher plants possess major nuclear gene-encoded extrinsic proteins named PsbO, PsbP, and PsbQ. PsbO is a common extrinsic protein highly conserved among the oxygenic phototrophs. PsbP and PsbQ are indigenous to plant PSII and have been proposed as the functional equivalents of PsbV and PsbU in bacterial PSII, having replaced them during the course of evolution from ancestral cyanobacteria to higher plants. These proteins play significant roles in the regulation and stabilization of the photosynthetic water oxidation [26, 27, 33] although the details of their function(s) are still a matter of debate.

In this chapter, I describe the structural-functional roles of extrinsic proteins in the plant PSII. The effects of extrinsic proteins on the photosynthetic function of the

Mn_4CaO_5 cluster and the structural stability of the OEC core complex were investigated by spectroscopic and biochemical analyses. Based on the results presented here and reported previously, the structural and functional roles of extrinsic proteins in the regulation and stabilization of photosynthetic functions are discussed.

3.2 Materials and methods

3.2.1 Sample preparation

In the present study, I used two types of PSII membranes lacking functional Ca^{2+} with or without extrinsic proteins (Ex) including PsbP and PsbQ as shown in Figure 3-1. BBY-type PS II membranes (untreated PSII, A) were prepared from spinach according to the method described previously [93]. The O_2-evolving activity was ~550 μmoles of O_2/mgChl/h. For depletion of Ca^{2+}, PsbP, and PsbQ, the membranes were suspended in medium A (2 M NaCl, 10 mM MES/NaOH, and pH 6.5) at 0.5 mg of Chl per ml and gently stirred on ice under weak light (10 μmol/s/m^2) for 30 min. Next, the following procedures were carried out in complete darkness or dim green light unless otherwise noted: EDTA was added to the suspension to achieve a final concentration of 1 mM, followed by 10-min incubation in the dark. The suspension was centrifuged and extensively washed with Chelex-treated medium B (400 mM sucrose, 20 mM NaCl, 20 mM MES/NaOH, and pH 6.5) to yield PSII membranes depleted of Ca^{2+}, PsbP, and PsbQ (ExCa^{2+}-depleted PSII, B). For depletion of PspP and PsbQ proteins, PS II membranes were suspended in medium A at 0.5 mg of Chl per ml, and gently stirred on ice in darkness for 30 min. The extracted PsbP and PsbQ proteins were reconstituted into the NaCl/EDTA-treated PSII to obtain Ca^{2+}-depleted PSII (C).

Alternatively, the PSII membranes were washed with medium C (400 mM sucrose, 20 mM NaC1, 0.1 mM MES-NaOH, and pH 6.5) and then treated with low –pH medium D (400 mM sucrose, 20 mM NaC1, 20 mM citrate-NaOH , pH 3.0) at 2 mg of Chl per ml. After 5 min incubation on ice in darkness, the suspension was diluted with medium D (400 mM sucrose, 20 mM NaC1, 500 mM MOPS-NaOH, pH 7.5), and incubated for 10 min to facilitate the rebinding of extrinsic proteins. Then,

the sample was washed with medium E (400 mM sucrose, 20 mM NaCl, 40 mM MES/NaOH, 0.5 mM EDTA, pH6.5) to obtain PSII membranes depleted of only Ca^{2+} (Low-pH-treated PSII, D). Finally, the resulting Low-pH-treated PSII membranes were treated with medium A to produce PSII membranes depleted of both Ca^{2+} and extrinsic proteins ($ExCa^{2+}$-depleted PSII, E).

3.2.2 O_2-evolving activity

O_2-evolving activities of the PSII preparations were measured at 25℃ with a Clark-type oxygen electrode in medium B (400 mM sucrose, 20 mM NaCl, 20 mM MES/NaOH, and pH 6.5) containing 20 mM $CaCl_2$ with 0.5 mM of phenyl-p-benzoquinone (PpBQ) as electron acceptor.

3.2.3 Pulse amplitude modulation (PAM) fluorescence measurement

The maximal photochemical quantum yield of PSII (F_v/F_m) was measured using a pulse-modulated fluorometer (Junior-PAM, Heinz Walz, Germany). The minimum fluorescence (F_0) was determined after a weak far red modulated light. Then the maximum fluorescence (F_m) was reached by exposing the sample suspension to a saturating light pulse. The maximum quantum yield of PS II (F_v/F_m) was calculated by the following equation.

$$F_v/F_m = (F_m - F_0)/F_m$$

3.2.4 ATR-FTIR spectroscopy

FTIR spectra were measured on an FTIR8600PC (SHIMADZU) spectrophotometer equipped with a ZnSe ATR optics. A solution of the extrinsic proteins (50~100 μl) with or without 5 to 10 mM of Ca^{2+} was dehydrated under a stream of dry air to form a dry film, and a single-beam spectrum (64 scans) for each film was recorded at 4 cm^{-1} resolution and room temperature.

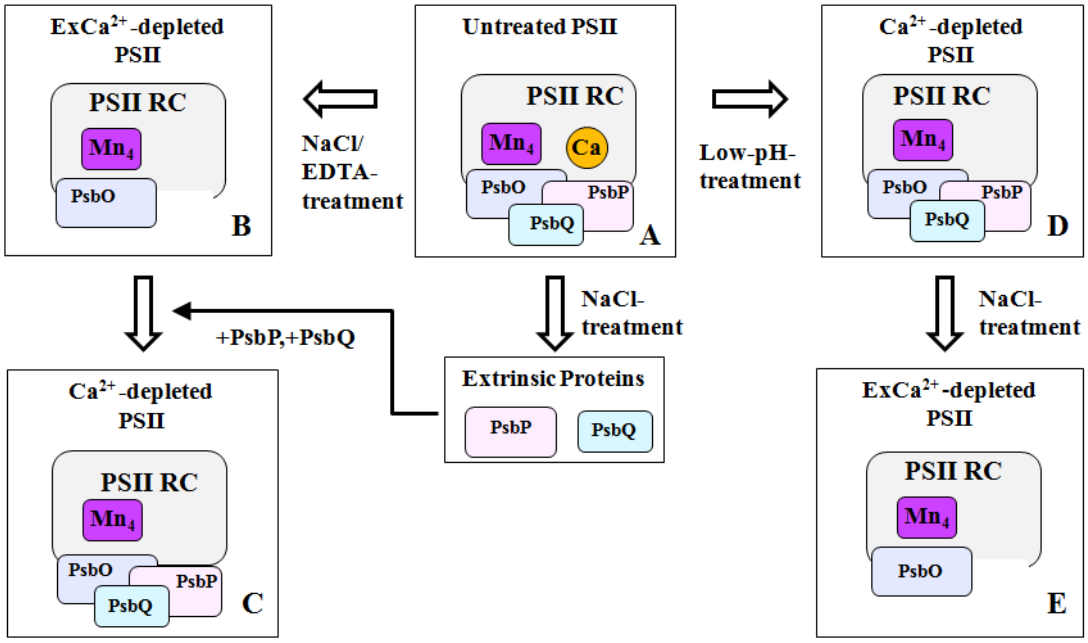

Figure 3-1. Schematic representation for the sample preparations of two types of PSII membranes lacking functional Ca^{2+} with or without PsbP and PsbQ.

3.3 Results and discussion

3.3.1 Interaction of extrinsic proteins with the Mn_4CaO_5 cluster in the OEC

The PSII membranes prepared by the different methods were assessed by O_2-evolving activity and Fv/Fm values of chlorophyll fluorescence and the resulting data are summarized in Table 3-1. The O_2-evolving rate of the untreated PSII was decreased to 17% when PsbP, PsbQ and Ca^{2+} were depleted by the NaCl/EDTA treatments (B). The decreased activity was restored to 83% by reconstituting Ca^{2+}, as reported previously [93, 94]. However, the addition of PsbP and PsbQ to the $ExCa^{2+}$-depleted PSII in the absence of Ca^{2+} lowered the O_2-evolving rate to ~0% (C). Furthermore, the O_2-evolving activity was almost completely lost upon Ca^{2+} depletion by the Low-pH treatment (D) but restored to 79% by adding Ca^{2+}. Notably, the lost activity was partially resotored by the further depletion of PsbP and PsbQ to 25% (E). These results indicate that PsbP and PsbQ proteins completely suppress O_2 evolution in the absence of functional Ca^{2+}. Similar effects are also evident in the chlorophyll fluorescence measurements: the Fv/Fm values were much lower in the Ca^{2+}-depleted PSII (45%) than in the $ExCa^{2+}$-depleted PSII (64%), and both values were recoverd to ~80% after the supplementation with Ca^{2+}. In the Ca^{2+}-depleted PSII, the partial recovery to 68% was induced by the following depletion of the extrinsic proteins. Since Fv/Fm values are related to O_2-evolving activity, this strongly suggests that the functions of the OEC are disturbed by the extrinsic proteins in the absence of Ca^{2+}.

Table 3-1. Effects of Ca^{2+} and extrinsic proteins (PsbP and PsbQ) on the properties of the OEC.

PSII preparation	Additives	O_2-evolving activity	Fv/Fm	FTIR S_2/S_1 carboxylate bands	Thermoluminescence Q-band (˚C)	S_2 EPR multiline signal
Untreated PSII (A)	No addition	100%	100%	Normal[b]	Normal[e,f]	Normal[f]
ExCa^{2+}-depleted PSII (B)	No addition	17%	64%	Normal[b]	Normal[b,d,e]	Normal[d]
	+Ca^{2+}	83%	79%	Normal[b]	Normal[b,d,e]	Normal[d]
	+PsbP, +PsbQ (C)	~0%	——[a]	——[a]	Abnormal[e]	Modified
	+PsbP	~0%	——[a]	——[a]	Abnormal[e,f]	——[a]
Ca^{2+}-depleted PSII (D)	No addition	~0%	45%	Abnormal[c]	Abnormal[e,f]	Modified[f]
	+Ca^{2+}	79%	81%	Normal[c]	Normal[e,f]	Normal[f]
	-PsbP, -PsbQ (E)	25%	68%	——[a]	Normal[e]	Normal

[a]Not reported, [b][93], [c][94], [d][92], [e][95], [f][46].

Next, the effects of extrinsic proteins and Ca^{2+} on the thermal stability of the OEC were examined. Figure 3-2 shows the relative absorbance at 680 nm of the untreated control PSII (circle), $ExCa^{2+}$-depleted (triangle), and Ca^{2+}-depleted (square) PSII membranes during incubation at 50˚C. The relative band intensity of the control PSII remained at ~85% after 64 min incubation, but was slightly decreased to ~75% in the $ExCa^{2+}$-depleted PSII and was markedly decreased to 50% in the Ca^{2+}-depleted PSII. This is consistent with the effects seen in the O_2-evolving activity and Fv/Fm values. These results strongly support the idea that PsbP and PsbQ lower the structural stability and disturb the normal functioning of the OEC in the absence of Ca^{2+}.

The present data are largely in agreement with previous findings, as shown in Table 3-1. FTIR spectroscopy provides valuable information on the structure and interactions within the OEC. The ligation geometry around the Mn_4CaO_5 cluster is mostly similar between untreated and $ExCa^{2+}$-depleted PSII, at least in the S_1- and S_2-states [94]. However, Ca^{2+}-depleted PSII exhibited marked deterioration in the carboxylate bands, which are thought to be from putative amino acid residues coordinating to the Mn_4CaO_5 cluster [95]. Furthermore, the redox potential of the Mn_4CaO_5 cluster has been reported to be abnormal when the extrinsic proteins bound to the PSII core in the absence of Ca^{2+}, as indicated by elevated peak temperatures of the thermoluminescence band for the $S_2Q_A^-$ recombination [46, 96]. Additional support for this view was obtained from electron paramagnetic resonance (EPR) studies which demonstrated abnormal magnetic structures of PSII lacking Ca^{2+} but retaining the extrinsic proteins as revealed by modified S_2-state multiline signals. These results are largely compatible with the present findings that the appropriate binding of extrinsic proteins in the presence of functional Ca^{2+} is required for the normal functioning of the OEC.

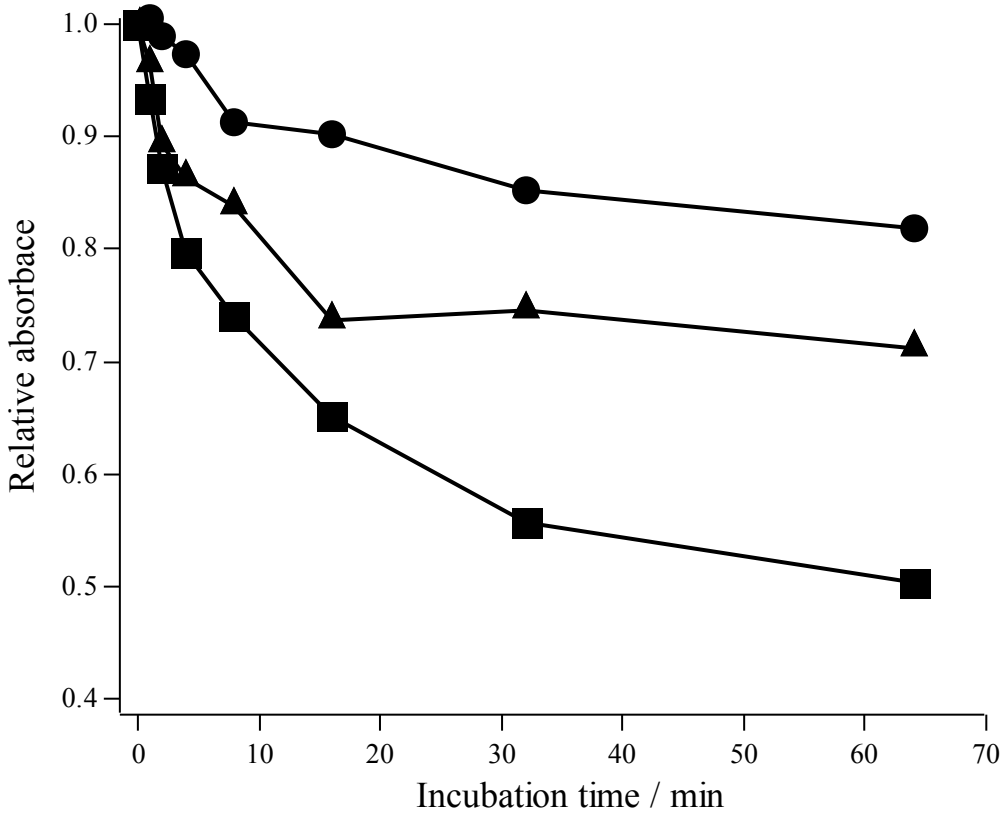

Figure 3-2. Plots of relative absorbance at 680 nm for the untreated (circle), $ExCa^{2+}$-depleted (triangle), and Ca^{2+}-depleted (square) PS II membranes as a function of incubation time at 50˚C.

To understand function of these extrinsic proteins in the OEC, structural changes of the PsbP and PsbQ proteins induced by Ca^{2+} were observed by ATR-FTIR spectroscopy. Figure 3-3 shows ATR-FTIR spectra of isolated PsbP and PsbQ (spectrum a) and those supplemented with Ca^{2+} (spectrum b). The control spectrum a exhibited characteristic bands for amide I (1700–1600 cm^{-1}) and amide II (1600–1500 cm^{-1}) vibrational modes from backbone polypeptides of the OEC. These bands were significantly modified when Ca^{2+} was added to the extrinsic proteins as can be clearly seen in the difference spectrum (lower part of Figure 3-3). The IR bands at 1693, 1659 and 1539 cm^{-1} are decreased and new bands are visible at 1641 and 1566 cm^{-1}, strongly indicating that PsbP and/or PsbQ are metal-binding proteins that alter their secondary structures upon the binding of Ca^{2+}. Similar structural changes were evident in the spectrum of the purified PsbP protein (Figure 3-4). Although high-resolution crystallographic studies have revealed the structure of the PsbP protein in *Nicotiana tabacum* [97], this protein lacks the N-terminal region which are thought to contain the Ca^{2+}-binding site, and therefore, the relationship between PsbP and Ca^{2+} remains unclear [98]. However, Bondarava et al. hypothesized that PsbP acts to reserve Mn^{2+} or Ca^{2+} ions [36]. These results strongly support the idea that the PsbP protein is a metal-binding protein that directly and/or indirectly interacts with the catalytic center of the OEC in the absence of sufficient Ca^{2+}.

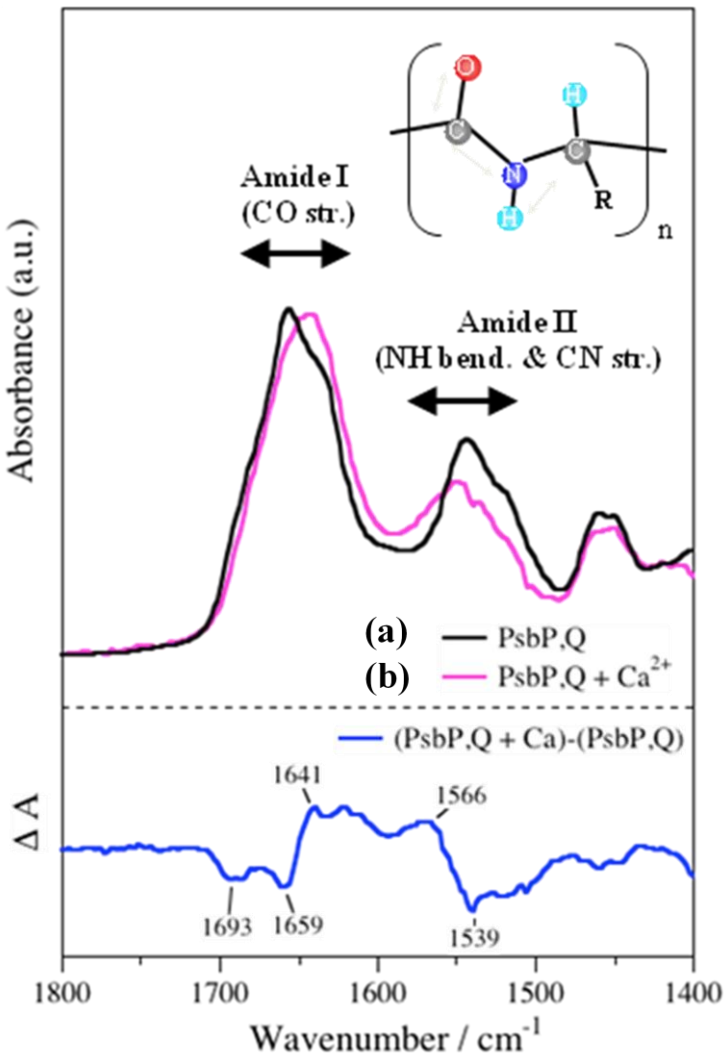

Figure 3-3. ATR-FTIR spectra of isolated PsbP and PsbQ proteins in the absence (a, black) and presence of Ca^{2+} (b, magenta). The difference spectrum obtained by subtracting spectrum a from spectrum b is shown in the lower panel.

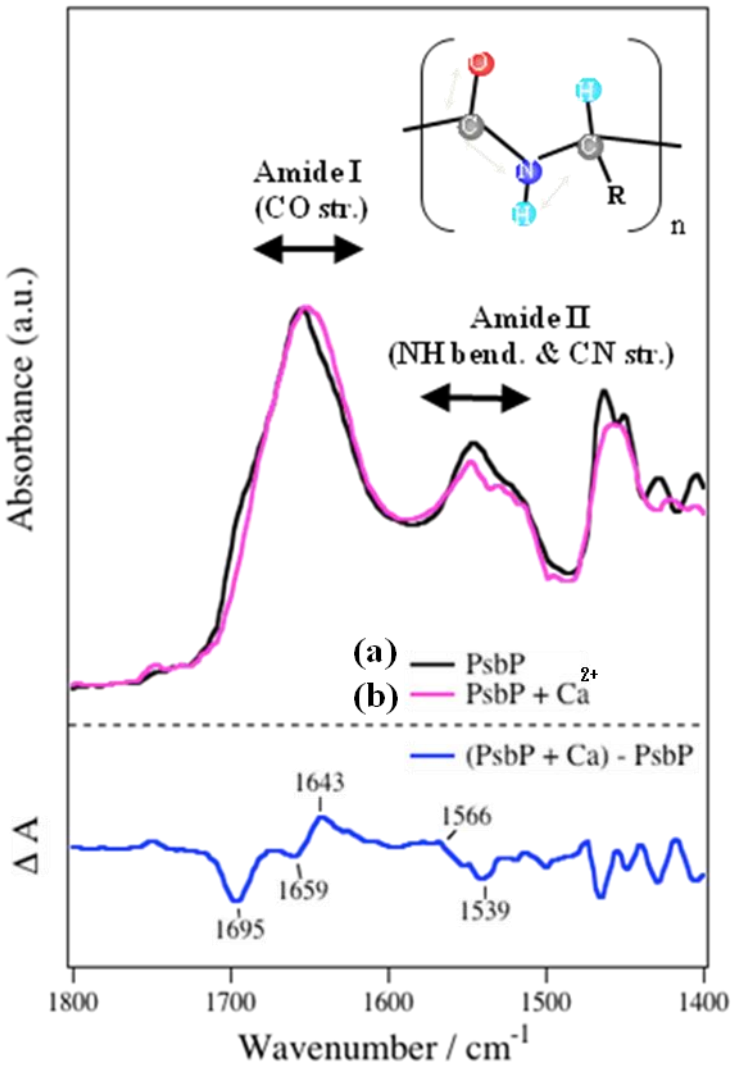

Figure 3-4. ATR-FTIR spectra of isolated PsbP proteins in the absence (a, black) and presence of Ca^{2+} (b, magenta). The difference spectrum obtained by subtracting spectrum a from spectrum b is shown in the lower panel.

The most important physiological role of PsbO is to stabilize the binding of the Mn_4CaO_5 cluster, which is essential for oxygen-evolving activity [53]. The PsbO protein can be dissociated from the PSII by a variety of chemical treatments including washing with alkaline Tris buffer, a high concentration of $CaCl_2$, and chaotropic agents [99, 100]. In particular, Lys residue-modifying chemicals such as *N*-succinimidyl propionate and 2,4,6-trinitrobenzene sulfonic acid caused release of PsbO from PSII and loss of oxygen-evolving activity [101], suggesting that the positive charge of Lys is important for the electrostatic interaction between PsbO and PSII. Alternatively, the release of PsbO can be caused by thermal denaturation. However, PsbO itself is a thermostable protein [102], and therefore, other factors might also be responsible for the release of PsbO as described later in this chapter.

Several spectroscopic studies using isolated PsbO reported different Ca^{2+}-binding properties between higher plants and cyanobacteria. It has been suggested that plant PsbO can bind Ca^{2+}, which induces slight changes in secondary structure from a β-sheet to a loop or disordered structure, and facilitated the association of PsbO with the PSII core [54, 55]. However, an EPR study indicated that the functional Ca^{2+} ion was not involved in the binding to PsbO [56]. In cyanobacteria, PsbO does not bind Ca^{2+}, at least before the protein associates with the PSII core, since no significant conformational change upon the Ca^{2+}-binding was induced in isolated PsbO [57]. In contrast, the low-affinity Ca^{2+}-binding site in PsbO located at the luminal exit of the proton channel has been suggested to be responsible for water oxidation [58, 59]. These results strongly indicate that the structural-functional role of PsbO is not identical between higher plants and cyanobacteria. Interestingly, thermal stability was enhanced when plant PsbO proteins were replaced with thermally stable homologues from thermophilic *Phormidium laminosum* [103]. Therefore, slight variation in the

primary structure and/or the protein folding pattern is possibly responsible for the difference in thermal stability of PsbO between higher plants and thermophilic cyanobacteria.

3.3.2 Protective role of extrinsic proteins in regulation and stabilization of photosynthetic functions

The present study revealed that PsbP significantly affects the structure and function of the Mn_4CaO_5 cluster in the OEC only in the absence of sufficient Ca^{2+} in the OEC. This result is compatible with the previous analyses that involved FTIR, thermoluminescence, and EPR spectoroscopies [46, 93-96]. In addition, it has been reported that PsbP has Ca^{2+}-binding sites in the N-terminal region [98] and functions as a reserver of Mn^{2+} or Ca^{2+} ions to supply them as needed by the impaired OEC [36]. Therefore, it is possible that the PsbP completely eliminates functional Ca^{2+} or interacts with the Mn_4CaO_5 cluster directly and/or indirectly to inhibit the O_2-evolving activity and modify the ligation geometry, redox potentials and magmetic structures of the Mn_4CaO_5 cluster.

It has been suggested that normal functioning of PSII requires 15 highly conserved residues in the N-terminal region of the PsbP protein as well as the PsbQ protein for retention of functional Ca^{2+} [104]. A recent FTIR study indicated that the PsbP protein, but not the PsbQ protein, has an effect on S_2/S_1 conformational changes of the intrisic polypeptide backbone around the Mn_4CaO_5 cluster through the N-terminal region of the PsbP [105]. In addition, little change was found in characteristic carboxylate stretching modes from putative amino acid ligands for the Mn_4CaO_5 cluster in the presence of Ca^{2+} when PsbP and PsbQ were depleted by NaCl washing, or all the extrinsic proteins were eliminated by $CaCl_2$ washing [105]. Based on these results, it is possible that the PsbP protein interacts with intrinsic proteins, which may be closely related to the Mn_4CaO_5 cluster, and preserves the OEC functions appropriately in the presence of Ca^{2+}, but modifies the properties of the cluster directly and/or indirectly through intrinsic proteins in the absence of Ca^{2+}.

It is intriguing to note that PsbV in cyanobacteria exhibits functional similarity with PsbP in higher plants, although their primary and 3D crystallographic structures are largely different [97, 106]. The apparent inconsistency in the structural-functional consequence may reflect the fact that PsbP and PsbV in plant and cyanobacterial PSII are not involved in specific interactions between the protein and the Mn_4CaO_5 cluster, but serve to maintain indispensable inorganic cofactors in the proximity of the cluster and to protect it from invasion of reductants. Additionally, PsbQ and PsbU also play a key role for tuning O_2-evolving activity and enahncing structural stability through the interaction with PsbP and PsbV, respectively [107, 108].

In higher plants, PSII is much more susceptible to high temperatures than PSI [109]. The thermal stability of the PSII core is closely related to the acquisition of cellular thermal tolerance in oxyphototrophs. The thermosensitivity of oxygen evolution in higher plants has been studied through simple experiments using PSII particles or isolated thylakoid membranes. Previous in-vivo and in-vitro studies have estimated the heat-labile properties of the OEC [109-111]. These studies demonstrated that the release of PsbO occurs first, followed by liberation of two of the four Mn^{2+} ions from the Mn_4CaO_5 cluster of the OEC [100, 112, 113], and finally by the loss of oxygen evolution at high temperatures [100, 114].

Another form of damage to the physiological function of the PSII can be caused by reactive oxygen species (ROS) generated under high light conditions. The D1 proteins are degraded by the ROS species and inhibited in their ability to repair the photodamaged PSII by suppressing the synthesis of D1 proteins [115]. The ROS are thought to arise from heat-induced inactivation of a water-oxidizing manganese complex and through lipid peroxidation [116]. On the other hand, saturation of polyunsaturated fatty acids (PUFAs) contributes to the acquisition of heat tolerance of

photosynthesis by altering physicochemical properties [117-119]. The increased saturation of PUFAs raises the temperature at which lipids phase-separate into non-bilayer structures, providing the proper assembly and dynamics of PSII tolerant to higher temperatures [120].

Recently, I reported biochemical evidence that the biological effect of reactive carbonyls such as malondialdehyde (MDA) and acrolein is greatly enhanced under heat-stressed conditions. [121]. PsbO is one of the proteins most frequently modified by MDA, which is an end-product of peroxidized polyunsaturated fatty acids. Detailed biochemical experiments indicated that the modification of PsbO by MDA affects its binding to the PSII complex and causes inactivation of the OEC (Figure 3-5). Purified PsbO and PSII membranes, from which extrinsic proteins had been eliminated, of the oxygen-evolving complex (PSIIΔOEE) of spinach were separately treated with MDA. The binding was diminished when both PsbO and PSIIΔOEE were modified, but when only PsbO or PSIIΔOEE was treated, the binding was not impaired. In an experiment using thylakoid membranes, the release of PsbO from PSII and a corresponding loss of oxygen-evolving activity were observed when thylakoid membranes were treated with MDA at 40°C but not at 25°C. In spinach leaves treated at 40°C under light, the maximum efficiency of PSII photochemistry (Fv/Fm ratio of chlorophyll fluorescence) and oxygen-evolving activity decreased. Simultaneously, the MDA content of the heat-stressed leaves increased, and PsbO and PSII core proteins (including 47 kDa and 43 kDa chlorophyll-binding proteins) were modified by MDA. In contrast, these changes were less profound when these experiments were performed at 40°C in the dark. Thus, MDA modification of PSII proteins likely causes the release of PsbO from PSII, an effect that is particularly marked in heat and oxidative conditions.

First, ROS attack trienoic fatty acids in thylakoid membranes, resulting in the generation of MDA. MDA attaches to critical Lys residues of PsbO and PsbB (CP47) for the interaction between PsbO and PSII in a temperature-dependent manner. When both sides of PsbO and PSII are modified by MDA, PsbO is released from PSII. Finally, the Mn_4CaO_5 cluster is spontaneously released from PSII, causing loss of oxygen-evolving activity.

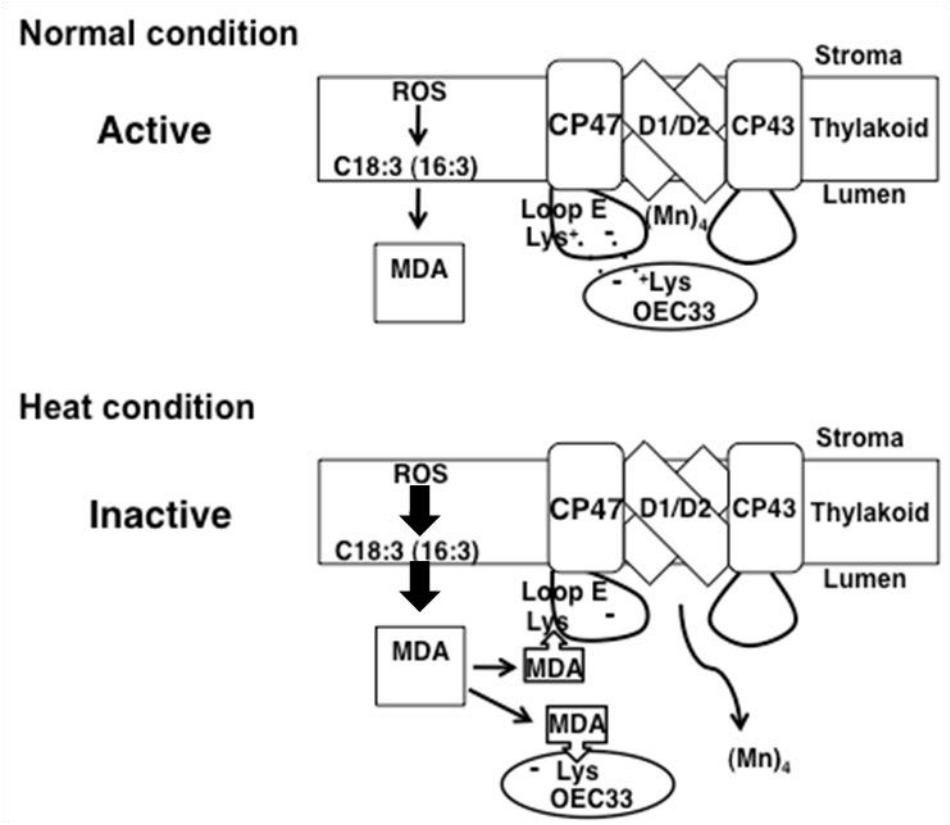

Figure 3-5. A schematic model of MDA-induced loss of oxygen evolution in heat-stressed spinach PSII complexes.

3.4 Conclusion

In this chapter, I focused on the structural and functional roles of extrinsic proteins in the plant PSII. Since PSII is an integrated pigment-protein complex embedded in plant membranes, the structures and interactions of these extrinsic proteins in the membrane interface are of significance for protecting the RC. This involves protecting the Mn_4CaO_5 cluster from exogenous invasion of reductants and/or alteration of physiological conditions. However, based on the results presented here and reported previously, I consider it very likely that the extrinsic protein itself is also responsible for the deterioration of the normal functioning of the OEC under inappropriate conditions. Further studies on the plant PSII, including high-resolution crystallographic studies, will be required for understanding the functions of extrinsic proteins in the structural stability and the water oxidation chemistry in PSII.

Chapter 4 Summary

In this doctoral dissertation, the structural and functional roles of calcium ions were investigated using photosynthetic organisms with type II RC. PSII is evolutionarily related to purple bacteria, as evidenced by the similarities in their heterodimeric RC and quinone-mediated electron transport system. The purple bacterial photosystem lacks Mn_4CaO_5 clusters, the catalytic center for the water oxidation, and certain extrinsic proteins which reside ubiquitously in the periphery of PSII. In purple bacteria, the circular pigment-protein complex known as LH1 is closely associated with the RC to maintain the structures and functions of the bacterial photosystem. Calcium ions are intimately related to the differences between the ancestral and evolved phototrophs with type-II reaction centers. Therefore, the roles of calcium are significant to understand how the photosynthetic organisms utilize calcium ions in response to their living environment and during the process of the evolution from the ancestral to evolved photosynthetic organisms with type-II reaction centers.

In Chapter 2, the structural and functional roles of calcium ions in purple bacteria, the ancestral photosynthetic organism with type-II reaction centers, were investigated. The light-harvesting 1 reaction center (LH1-RC) complex from purple sulfur photosynthetic bacterium *Tch. tepidum* is believed to enhance thermal stability by binding of Ca^{2+} to the C-terminus of the LH1-polypeptides. However, structural roles of Ca^{2+} and details of the Ca^{2+}-binding site are remained to be resolved. Here, I applied perfusion-induced ATR-FTIR spectroscopy to highly purified LH1-RC complexes from *Tch. tepidum*, and detected for the first time metal-sensitive fine structural changes involved in the enhanced thermal stability of this complex. The *Tch. tepidum* LH1-RC complex exhibited Sr^{2+}/Ca^{2+} ATR-FTIR difference bands that

reflect changes of polypeptide backbones and amino acid residues upon the replacement of native Ca^{2+} with Sr^{2+}. The difference bands also appeared in the following Ca^{2+}/Sr^{2+} difference spectra with almost identical intensities but inverse signs, demonstrating that the structural changes induced by the metal exchange are fully reversible. In contrast, these ATR-FTIR signals were faintly detected in the mesophilic counterpart, *Alc. vinosum*. A comparative analysis using LH1 complexes lacking the RCs strongly indicated that the metal-sensitive bands originate from polypeptide backbones and amino acid residues near the putative Ca^{2+}-binding site at the C-terminal region of *Tch. tepidum* LH1 complexes. Structural changes induced by Sr^{2+}- and Ba^{2+}-substitutions were essentially identical. However, Cd^{2+}-substitution exhibited unique structural modifications, which may be responsible for the severely deteriorated thermal stability of Cd^{2+}-substituted complexes. Furthermore, the observed FTIR signals were tentatively assigned based on the isotopic shifts by uniform ^{15}N, ^{13}C and ^{2}H-labelings of LH1-RC complexes. The molecular mechanism enhancing the thermal stability of *Tch. tepidum* LH1-RC proteins is proposed based on the possible assignments of the ATR-FTIR signals and the recent structural information on the Ca^{2+}-binding site.

In Chapter 3, the structural and functional roles of calcium ions in PS II from higher plants, the evolved photosynthetic organism with type-II reaction centers, were discussed in connection with the extrinsic proteins that are lacking in the ancestral purple bacteria. Photosynthetic oxygen evolution occurs in an OEC of PSII although details of the reaction mechanism are not fully understood. It is known that one OEC includes one or two Ca^{2+}, depletion of which results in the loss of oxygen-evolving ability. In addition, an extrinsic protein PsbP is closely related with binding properties of the functional Ca^{2+}. Therefore, it is significant to understand functional and

structural roles of Ca^{2+} and extrinsic proteins for elucidating the reaction mechanism of the photosynthetic oxygen evolution. In the present study, effects of depletion of Ca^{2+} and/or extrinsic proteins from the PSII on the oxygen-evolving ability, pulse amplitude modulation fluorescence measurement, and thermal stability of the OEC were examined using Ca^{2+}-depleted PSII samples prepared by different biochemical procedures. The oxygen-evolving activity of NaCl/EDTA preparation in which Ca^{2+} and extrinsic proteins (PsbP, PsbQ) are depleted was decreased to ~20% compared with untreated preparations. On the other hand, the oxygen evolution was completely a suppressed when only Ca^{2+} was removed from the PSII by Low-pH treatment. In addition, Low-pH preparation was less stable than NaCl/EDTA preparation. Based on these findings, I proposed that the extrinsic protein, particularly PsbP, plays a significant role to protect the OEC in the presence of Ca^{2+}, whereas the PsbP may act as a metal-binding protein in the absence of Ca^{2+} to decompose the catalytic Mn_4CaO_5 cluster, resulting in the loss of O_2-evolving activity and the deterioration of the structural stability.

Acknowledgments

Firstly, I would like to express my sincere appreciation to my adviser, Professor Takashi Ohno (Graduate School of Agricultural Science, Kobe University) for giving me this precious opportunity to take the degree of Doctor of Agriculture in his laboratory. I especially would like to express my deepest appreciation to my supervisor, Assistant Professor Yukihiro Kimura for his elaborated guidance, considerable encouragement and invaluable discussion that make my research of great achievement.

I would like to express my gratitude to thesis committee members, Professor Yukihiro Sugimoto (Graduate School of Agricultural Science, Kobe University) and Associate Professor Kengo Kanamaru (Graduate School of Agricultural Science, Kobe University) for their through reviews and valuable comments on this thesis.

I wish to express earnest thankfulness to Professor Zheng-Yu Wang-Otomo (Faculty of Science, Ibaraki University) and Professor Taka-aki Ono (Graduate School of Engineering Faculty Engineering, Ibaraki University) for their valuable advice and cooperation. I thank to Assistant Professor Yasuo Yamauchi (Graduate School of Agricultural Science, Kobe University) for his technical support during this study.

Finally, I am very grateful to Mr. Yuki Yura for his valuable cooperation in my experiments. I also express my deep gratitude to all the members of Ohno laboratory at Kobe University for their encouragement.

References

[1] R.J. Cogdell, A. Gall, J. Kohler, The architecture and function of the light-harvesting apparatus of purple bacteria: from single molecules to *in vivo* membranes, Q. Rev. Biophys. 39 (2006) 227-324.

[2] J. Deisenhofer, O. Epp, K. Miki, R. Huber, H. Michel, X-ray Structure Analysis of a Membrane Protein Complex Electron Density Map at 3Å Resolution and a Model of the Chromophores of the Photosynthetic Reaction Center from *Rhodopseudomonas viridis*, J. Mol. Biol. 180 (1984) 385-398.

[3] J.P. Allen, G. Feher, T.O. Yeates, D.C. Rees, J. Deisenhofer, H. Michel, R. Huber, Structural Homology of Reaction Centers from *Rhodopseudomonas Sphaeroides* and *Rhodopseudomonas Viridis* as Determined by X-ray Diffraction, Proc. Natl. Acad. Sci. U. S. A. 83 (1986) 8589-8593.

[4] T. Nogi, I. Fathir, M. Kobayashi, T. Nozawa, K. Miki, Crystal structures of photosynthetic reaction center and high-potential iron-sulfur protein from *Thermochromatium tepidum*: Thermostability and electron transfer, Proc. Natl. Acad. Sci. U. S. A. 97 (2000) 13561-13566.

[5] A.W. Roszak, T.D. Howard, J. Southall, A.T. Gardiner, C.J. Law, N.W. Isaacs, R.J. Cogdell, Crystal Structure of the RC-LH1 Core Complex from *Rhodopseudomonas palustris*, Science 302 (2003) 1969-1972.

[6] S. Karrasch, P.A. Bullough, R. Ghosh, The 8.5Å Projection Map of the Light-Harvesting Complex I from *Rhodospirillum rubrum* Reveals a Ring Composed of 16 Subunits, EMBO J. 14 (1995) 631-638.

[7] S.J. Jamieson, P.Y. Wang, P. Qian, J.Y. Kirkland, M.J. Conroy, C.N. Hunter, P.A. Bullough, Projection structure of the photosynthetic reaction centre-antenna

complex of *Rhodospirillum rubrum* at 8.5 Å resolution, EMBO J. 21 (2002) 3927-3935.

[8] D. Fotiadis, P. Qian, A. Philippsen, P.A. Bullough, A. Engel, C.N. Hunter, Structural analysis of the reaction center light-harvesting complex I photosynthetic core complex of *Rhodospirillum rubrum* using atomic force microscopy, J. Biol. Chem. 279 (2004) 2063-2068.

[9] S. Scheuring, F. Francia, J. Busselez, B.A. Melandri, J.L. Rigaud, D. Levy, Structural role of PufX in the dimerization of the photosynthetic core complex of *Rhodobacter sphaeroides*, J. Biol. Chem. 279 (2004) 3620-3626.

[10] P. Qian, C.N. Hunter, P.A. Bullough, The 8.5 Å Projection Structure of the Core RC-LH1-PufX Dimer of *Rhodobacter sphaeroides*, J. Mol. Biol. 349 (2005) 948-960.

[11] S. Scheuring, J. Busselez, D. Levy, Structure of the dimeric PufX-containing core complex of *Rhodobacter blasticus* by *in situ* atomic force microscopy, J. Biol. Chem. 280 (2005) 1426-1431.

[12] Y. Kimura, Y. Hirano, L.J. Yu, H. Suzuki, M. Kobayashi, Z.Y. Wang, Calcium ions are involved in the unusual red shift of the light-harvesting 1 Q_y transition of the core complex in thermophilic purple sulfur bacterium *Thermochromatium tepidum*, J. Biol. Chem. 283 (2008) 13867-13873.

[13] F. Ma, Y. Kimura, X.H. Zhao, Y.S. Wu, P. Wang, L.M. Fu, Z.Y. Wang, J.P. Zhang, Excitation dynamics of two spectral forms of the core complexes from photosynthetic bacterium Thermochromatium tepidum, Biophys. J. 95 (2008) 3349-3357.

[14] A. Zouni, H.T. Witt, J. Kern, P. Fromme, N. Krauss, W. Saenger, P. Orth, Crystal structure of photosystem II from *Synechococcus elongatus* at 3.8 Å resolution,

Nature 409 (2001) 739-743.

[15] N. Kamiya, J.R. Shen, Crystal structure of oxygen-evolving photosystem II from Thermosynechococcus vulcanus at 3.7-Å resolution, Proc. Natl. Acad. Sci. U. S. A. 100 (2003) 98-103.

[16] K.N. Ferreira, T.M. Iverson, K. Maghlaoui, J. Barber, S. Iwata, Architecture of the photosynthetic oxygen-evolving center, Science 303 (2004) 1831-1838.

[17] B. Loll, J. Kern, W. Saenger, A. Zouni, J. Biesiadka, Towards complete cofactor arrangement in the 3.0 Å resolution structure of photosystem II, Nature 438 (2005) 1040-1044.

[18] A. Guskov, J. Kern, A. Gabdulkhakov, M. Broser, A. Zouni, W. Saenger, Cyanobacterial photosystem II at 2.9-Å resolution and the role of quinones, lipids, channels and chloride, Nature Structural & Molecular Biology 16 (2009) 334-342.

[19] Y. Umena, K. Kawakami, J.R. Shen, N. Kamiya, Crystal structure of oxygen-evolving photosystem II at a resolution of 1.9 Å, Nature 473 (2011) 55-U65.

[20] P. Joliot, G. Barbieri, R. Chabaud, A New Model of Photochemical Centers in System-2, Photochem. Photobiol. 10 (1969) 309-&.

[21] B. Kok, B. Forbush, M. McGloin, Cooperation of charges in photosynthetic O_2 evolution-I. A linear four step mechanism, Photochem. Photobiol. 11 (1970) 457-475.

[22] A. Gabdulkhakov, A. Guskov, M. Broser, J. Kern, F. Muh, W. Saenger, A. Zouni, Probing the Accessibility of the Mn_4Ca Cluster in Photosystem II: Channels Calculation, Noble Gas Derivatization, and Cocrystallization with DMSO, Structure 17 (2009) 1223-1234.

[23] J. Nield, M. Balsera, J. De Las Rivas, J. Barber, Three-dimensional electron cryo-microscopy study of the extrinsic domains of the oxygen-evolving complex of spinach - Assignment of the PsbO protein, J. Biol. Chem. 277 (2002) 15006-15012.

[24] J. Nield, J. Barber, Refinement of the structural model for the Photosystem II supercomplex of higher plants, Bba-Bioenergetics 1757 (2006) 353-361.

[25] J. De Las Rivas, M. Balsera, J. Barber, Evolution of oxygenic photosynthesis: genome-wide analysis of the OEC extrinsic proteins, Trends in Plant Science 9 (2004) 18-25.

[26] J.L. Roose, K.M. Wegener, H.B. Pakrasi, The extrinsic proteins of photosystem II, Photosynth Res 92 (2007) 369-387.

[27] A.K. Williamson, Structural and functional aspects of the MSP (PsbO) and study of its differences in thermophilic versus mesophilic organisms, Photosynth Res 98 (2008) 365-389.

[28] M. Miyao, N. Murata, Partial Reconstitution of the Photosynthetic Oxygen Evolution System by Rebinding of the 33-kDa Polypeptide, FEBS Lett. 164 (1983) 375-378.

[29] M. Miyao, N. Murata, The Mode of Binding of 3 Extrinsic Proteins of 33 kDa, 23 kDa and 18 kDa in the Photosystem II Complex of Spinach, Biochim. Biophys. Acta 977 (1989) 315-321.

[30] M. Miyao, N. Murata, Partial Disintegration and Reconstitution of the Photosynthetic Oxygen Evolution System - Binding of 24 Kilodalton and 18 Kilodalton Polypeptides, Biochemical Et Biophysica Acta 725 (1983) 87-93.

[31] A. Tohri, N. Dohmae, T. Suzuki, H. Ohta, Y. Inoue, I. Enami, Identification of domains on the extrinsic 23 kDa protein possibly involved in electrostatic

interaction with the extrinsic 33 kDa protein in spinach photosystem II, Eur. J. Biochem. 271 (2004) 962-971.

[32] K. Ifuku, S. Ishihara, R. Shimamoto, K. Ido, F. Sato, Structure, function, and evolution of the PsbP protein family in higher plants, Photosynth Res 98 (2008) 427-437.

[33] A. Seidler, The extrinsic polypeptides of Photosystem II, Bba-Bioenergetics 1277 (1996) 35-60.

[34] G. Renger, T. Renger, Photosystem II: The machinery of photosynthetic water splitting, Photosynth Res 98 (2008) 53-80.

[35] K. Ifuku, Y. Yamamoto, T. Ono, S. Ishihara, F. Sato, PsbP protein, but not PsbQ protein, is essential for the regulation and stabilization of photosystem II in higher plants, Plant Physiol. 139 (2005) 1175-1184.

[36] N. Bondarava, P. Beyer, A. Krieger-Liszkay, Function of the 23 kDa extrinsic protein of photosystem II as a manganese binding protein and its role in photoactivation, Bba-Bioenergetics 1708 (2005) 63-70.

[37] M. Balsera, J.B. Arellano, J.L. Revuelta, J. de las Rivas, J.A. Hermoso, The 1.49 Å resolution crystal structure of PsbQ from photosystem II of Spinacia oleracea reveals a PPII structure in the N-terminal region, J. Mol. Biol. 350 (2005) 1051-1060.

[38] X.P. Yi, S.R. Hargett, L.K. Frankel, T.M. Bricker, The PsbQ protein is required in Arabidopsis for photosystem II assembly/stability and photoautotrophy under low light conditions, J. Biol. Chem. 281 (2006) 26260-26267.

[39] N. Kamiya, K. Kawakami, Y. Umena, J.R. Shen, Structure of the catalytic, inorganic core of oxygen-evolving photosystem II at 1.9 Å resolution, J Photoch Photobio B 104 (2011) 9-18.

[40] Y. Kimura, L.J. Yu, Y. Hirano, H. Suzuki, Z.Y. Wang, Calcium ions are required for the enhanced thermal stability of the light-harvesting-reaction center core complex from thermophilic purple sulfur bacterium *Thermochromatium tepidum*, J. Biol. Chem. 284 (2009) 93-99.

[41] Y. Kimura, Y. Inada, L.J. Yu, Z.Y. Wang, T. Ohno, A Spectroscopic Variant of the Light-Harvesting 1 Core Complex from the Thermophilic Purple Sulfur Bacterium *Thermochromatium tepidum*, Biochemistry 50 (2011) 3638-3648.

[42] Y. Kimura, Y. Inada, T. Numata, T. Arikawa, Y. Li, J.P. Zhang, Z.Y. Wang, T. Ohno, Metal cations modulate the bacteriochlorophyll-protein interaction in the light-harvesting 1 core complex from *Thermochromatium tepidum*, Biochim. Biophys. Acta 1817 (2012) 1022-1029.

[43] Z.Y. Wang, M. Shimonaga, H. Suzuki, M. Kobayashi, T. Nozawa, Purification and characterization of the polypeptides of core light-harvesting complexes from purple sulfur bacteria, Photosynth Res 78 (2003) 133-141.

[44] L.J. Yu, S. Kato, Z.Y. Wang, Examination of the putative Ca^{2+}-binding site in the light-harvesting complex 1 of thermophilic purple sulfur bacterium *Thermochromatium tepidum*, Photosynth Res (in press).

[45] R.J. Debus, The Manganese and Calcium Ions of Photosynthetic Oxygen Evolution, Biochim. Biophys. Acta 1102 (1992) 269-352.

[46] T.A. Ono, Y. Inoue, Roles of Ca^{2+} in O_2 Evolution in Higher Plant Photosystem II: Effects of Replacement of Ca^{2+} Site by Other Cations, Arch. Biochem. Biophys. 275 (1989) 440-448.

[47] A. Boussac, J.L. Zimmermann, A.W. Rutherford, Epr Signals from Modified Charge Accumulation States of the Oxygen Evolving Enzyme in Ca^{2+} Deficient Photosystem II, Biochemistry 28 (1989) 8984-8989.

[48] D.F. Ghanotakis, G.T. Babcock, C.F. Yocum, Calcium Reconstitutes High-Rates of Oxygen Evolution in Polypeptide Depleted Photosystem II Preparations, FEBS Lett. 167 (1984) 127-130.

[49] A. Boussac, A.W. Rutherford, Nature of the Inhibition of the Oxygen-Evolving Enzyme of Photosystem II Induced by NaCl Washing and Reversed by the Addition of Ca^{2+} or Sr^{2+}, Biochemistry 27 (1988) 3476-3483.

[50] J. Matysik, Alia, G. Nachtegaal, H.J. van Gorkom, A.J. Hoff, H.J.M. de Groot, Exploring the Calcium-Binding Site in Photosystem II Membranes by Solid-State ^{113}Cd NMR, Biochemistry 39 (2000) 6751-6755.

[51] P.J. Booth, A.W. Rutherford, A. Boussac, Location of the calcium binding site in Photosystem II: A Mn^{2+} substitution study, Bba-Bioenergetics 1277 (1996) 127-134.

[52] H.A. Chu, A.P. Nguyen, R.J. Debus, Amino-Acid-Residues That Influence the Binding of Manganese or Calcium to Photosystem II. 1. The Lumenal Interhelical Domains of the D1 Polypeptide, Biochemistry 34 (1995) 5839-5858.

[53] R.J. Debus, Amino acid residues that modulate the properties of tyrosine Y_Z and the manganese cluster in the water oxidizing complex of photosystem II, Bba-Bioenergetics 1503 (2001) 164-186.

[54] P. Heredia, J. De Las Rivas, Calcium-dependent conformational change and thermal stability of the isolated PsbO protein detected by FTIR Spectroscopy, Biochemistry 42 (2003) 11831-11838.

[55] J. Kruk, K. Burda, M. Jemiola-Rzeminska, K. Strzalka, The 33 kDa Protein of Photosystem II is a Low-Affinity Calcium- and Lanthanide-Binding Protein, Biochemistry 42 (2003) 14862-14867.

[56] A. Seidler, A.W. Rutherford, The role of the extrinsic 33 kDa protein in Ca^{2+}

binding in photosystem II, Biochemistry 35 (1996) 12104-12110.

[57] B. Loll, G. Gerold, D. Slowik, W. Voelter, C. Jung, W. Saenger, K.D. Irrgang, Thermostability and Ca^{2+} binding properties of wild type and heterologously expressed PsbO protein from cyanobacterial photosystem II, Biochemistry 44 (2005) 4691-4698.

[58] A.W. Rutherford, P. Faller, The heart of photosynthesis in glorious 3D, Trends Biochem. Sci. 26 (2001) 341-344.

[59] J.W. Murray, J. Barber, Identification of a calcium-binding site in the PsbO protein of photosystem II, Biochemistry 45 (2006) 4128-4130.

[60] J.R. Shen, M. Qian, Y. Inoue, R.L. Burnap, Functional Characterization of *Synechocystis* sp. PCC 6803 Δ*psb*U and Δ *psb*V Mutants Reveals Important Roles of Cytochrome c-550 in Cyanobacterial Oxygen Evolution, Biochemistry 37 (1998) 1551-1558.

[61] J.R. Shen, Y. Inoue, Binding and functional properties of two new extrinsic components, cytochrome c-550 and a 12 kDa protein, in cyanobacterial photosystem II, Biochemistry 32 (1993) 1825-1832.

[62] Y. Nishiyama, H. Hayashi, T. Watanabe, N. Murata, Photosynthetic Oxygen Evolution Is Stabilized by Cytochrome C_{550} against Heat Inactivation in Synechococcus sp. PCC 7002, Plant Physiol. 105 (1994) 1313-1319.

[63] J.R. Shen, R.L. Burnap, Y. Inoue, An Independent Role of Cytochrome C-550 in Cyanobacterial Photosystem II as Revealed by Double-Deletion Mutagenesis of the Psbo and Psbv Genes in Synechocystis Sp Pcc-6803, Biochemistry 34 (1995) 12661-12668.

[64] J.R. Shen, W. Vermaas, Y. Inoue, The Role of Cytochrome c-550 as Studied through Reverse Genetics and Mutant Characterization in *Synechocystis* sp. PCC

6803, J. Biol. Chem. 270 (1995) 6901-6907.

[65] S. Scheuring, J. Seguin, S. Marco, D. Levy, B. Robert, J.L. Rigaud, Nanodissection and high-resolution imaging of the *Rhodopseudomonas viridis* photosynthetic core complex in native membranes by AFM, Proc. Natl. Acad. Sci. U. S. A. 100 (2003) 1690-1693.

[66] M.T. Madigan, A Novel Photosynthetic Purple Bacterium Isolated from a Yellowstone Hot-Spring, Science 225 (1984) 313-315.

[67] M.T. Madigan, Anoxygenic phototrophic bacteria from extreme environments, Photosynth Res 76 (2003) 157-171.

[68] M. Kobayashi, Y. Fujioka, T. Mori, M. Terashima, H. Suzuki, Y. Shimada, T. Saito, Z.Y. Wang, T. Nozawa, Reconstitution of photosynthetic reaction centers and core antenna-reaction center complexes in liposomes and their thermal stability, Biosci Biotech Bioch 69 (2005) 1130-1136.

[69] A.J. Watson, A.V. Hughes, P.K. Fyfe, M.C. Wakeham, K. Holden-Dye, P. Heathcote, M.R. Jones, On the role of basic residues in adapting the reaction centre - LH1 complex for growth at elevated temperatures in purple bacteria, Photosynth Res 86 (2005) 81-100.

[70] L.J. Yu, S. Kato, Z.Y. Wang, Examination of the putative Ca^{2+}-binding site in the light-harvesting complex 1 of thermophilic purple sulfur bacterium *Thermochromatium tepidum*, Photosynth Res 106 (2010) 215-220.

[71] J. Guijarro, M. Engelhard, F. Siebert, Anion Uptake in Halorhodopsin from *Natromonas pharaonis* Studied by FTIR Spectroscopy: Consequences for the Anion Transport Mechanism, Biochemistry 45 (2006) 11578-11588.

[72] P.R. Rich, J. Breton, Attenuated total Reflection Fourier Transform Infrared Studies of Redox Changes in Bovine Cytochrome *c* Oxidase: Resolution of the

Redox Fourier Transform Infrared Difference Spectrum of Heme a_3, Biochemistry 41 (2002) 967-973.

[73] A. Barth, C. Zscherp, What vibrations tell us about proteins, Q. Rev. Biophys. 35 (2002) 369-430.

[74] F. Ma, Y. Kimura, L.J. Yu, P. Wang, X.C. Ai, Z.Y. Wang, J.P. Zhang, Specific Ca^{2+}-binding motif in the LH1 complex from photosynthetic bacterium *Thermochromatium tepidum* as revealed by optical spectroscopy and structural modeling, Febs J 276 (2009) 1739-1749.

[75] H. Suzuki, Y. Hirano, Y. Kimura, S. Takaichi, M. Kobayashi, K. Miki, Z.Y. Wang, Purification, characterization and crystallization of the core complex from thermophilic purple sulfur bacterium *Thermochromatium tepidum*, Biochim. Biophys. Acta 1767 (2007) 1057-1063.

[76] T. Nozawa, J.T. Trost, T. Fukada, M. Hatano, J.D. Mcmanus, R.E. Blankenship, Properties of the Reaction Center of the Thermophilic Purple Photosynthetic Bacterium Chromatium-Tepidum, Biochim. Biophys. Acta 894 (1987) 468-476.

[77] A. Marechal, M. Iwaki, P.R. Rich, Structural Changes in Cytochrome c Oxidase Induced by Binding of Sodium and Calcium Ions: An ATR-FTIR Study, J. Am. Chem. Soc. 135 (2013) 5802-5807.

[78] H.P. Permentier, S. Neerken, J. Overmann, J. Amesz, A bacteriochlorophyll a antenna complex from purple bacteria absorbing at 963 nm, Biochemistry 40 (2001) 5573-5578.

[79] O. Rucker, A. Kohler, B. Behammer, K. Sichau, J. Overmann, *Puf* operon sequences and inferred structures of light-harvesting complexes of three closely related *Chromatiaceae* exhibiting different absorption characteristics, Arch. Microbiol. 194 (2012) 123-134.

[80] Z.-Y. Wang-Otomo, L.-J. Yu, S. Niwa, K. Takeda, Y. Hirano, T. Kawakami, K. Miki, Crystal structure of a LH1-RC core complex from *Thermochromatium tepidum*, The 16th International Congress on Photosynthesis (2013).

[81] Y. Kimura, N. Mizusawa, A. Ishii, T. Yamanari, T.A. Ono, Changes of low-frequency vibrational modes induced by universal ^{15}N- and ^{13}C-isotope labeling in S_2/S_1 FTIR difference spectrum of oxygen-evolving complex, Biochemistry 42 (2003) 13170-13177.

[82] T. Noguchi, M. Sugiura, Analysis of flash-induced FTIR difference spectra of the S-state cycle in the photosynthetic water-oxidizing complex by uniform ^{15}N and ^{13}C- isotope labeling, Biochemistry 42 (2003) 6035-6042.

[83] H. Suzuki, M. Sugiura, T. Noguchi, FTIR study on the proton release pattern during water oxidation in Photosystem II core complexes from Thermosynechococcus elongatus, Photosynth Res 91 (2007) 182-182.

[84] G. Socrates, Infrared and Raman characteristic group frequencies : tables and charts, 3rd ed., Wiley, Chichester ; New York, 2001.

[85] G.B. Deacon, R.J. Phillips, Relationships between the Carbon-Oxygen Stretching Frequencies of Carboxylato Complexes and the Type of Carboxylate Coordination, Coordin Chem Rev 33 (1980) 227-250.

[86] K. Nakamoto, Infrared and Raman Spectra of Inorganic and Coordination Compounds, Part B: Applications in Coordination, Organometallic, and Bioinorganic Chemistry, 5th ed., John Wiley & Sons, New York, 1997.

[87] S.Y. Venyaminov, N.N. Kalnin, Quantitative Ir Spectrophotometry of Peptide Compounds in Water (H_2O) Solutions. 2. Amide Absorption-Bands of Polypeptides and Fibrous Proteins in Alpha-Coil, Beta-Coil, and Random Coil Conformations, Biopolymers 30 (1990) 1259-1271.

[88] S.Y. Venyaminov, N.N. Kalnin, Quantitative Ir Spectrophotometry of Peptide Compounds in Water (H_2O) Solutions. 1. Spectral Parameters of Amino-Acid Residue Absorption-Bands, Biopolymers 30 (1990) 1243-1257.

[89] J.D. Olsen, G.D. Sockalingum, B. Robert, C.N. Hunter, Modification of a Hydrogen-Bond to a Bacteriochlorophyll-a Molecule in the Light-Harvesting 1 Antenna of *Rhodobacter sphaeroides*, Proc. Natl. Acad. Sci. U. S. A. 91 (1994) 7124-7128.

[90] J.N. Sturgis, J.D. Olsen, B. Robert, C.N. Hunter, Functions of conserved tryptophan residues of the core light-harvesting complex of *Rhodobacter sphaeroides*, Biochemistry 36 (1997) 2772-2778.

[91] E. Nabedryk, K.A. Bagley, D.L. Thibodeau, M. Bauscher, W. Mantele, J. Breton, A Protein Conformational Change Associated with the Photoreduction of the Primary and Secondary Quinones in the Bacterial Reaction Center, FEBS Lett. 266 (1990) 59-62.

[92] J.P. McEvoy, G.W. Brudvig, Water-Splitting Chemistry of Photosystem II, Chem. Rev. 106 (2006) 4455-4483.

[93] T. Ono, A. Rompel, H. Mino, N. Chiba, Ca^{2+} function in photosynthetic oxygen evolution studied by alkali metal cations substitution, Biophys. J. 81 (2001) 1831-1840.

[94] Y. Kimura, T. Ono, Chelator-induced disappearance of carboxylate stretching vibrational modes in S_2/S_1 FTIR spectrum in oxygen-evolving complex of photosystem II, Biochemistry 40 (2001) 14061-14068.

[95] T. Noguchi, T. Ono, Y. Inoue, Direct Detection of a Carboxylate Bridge between Mn and Ca^{2+} in the Photosynthetic Oxygen-Evolving Center by Means of Fourier-Transform Infrared-Spectroscopy, Bba-Bioenergetics 1228 (1995)

189-200.

[96] T.A. Ono, S. Izawa, Y. Inoue, Structural and Functional Modulation of the Manganese Cluster in Ca^{2+}-Depleted Photosystem II Induced by Binding of the 24-Kilodalton Extrinsic Protein, Biochemistry 31 (1992) 7648-7655.

[97] K. Ifuku, T. Nakatsu, H. Kato, F. Sato, Crystal structure of the PsbP protein of photosystem II from Nicotiana tabacum, Embo Reports 5 (2004) 362-367.

[98] K. Ifuku, F. Sato, A truncated mutant of the extrinsic 23-kDa protein that absolutely requires the extrinsic 17-kDa protein for Ca^{2+} retention in photosystem II, Plant Cell Physiol. 43 (2002) 1244-1249.

[99] D.F. Ghanotakis, C.F. Yocum, Photosystem II and the Oxygen-Evolving Complex, Annu Rev Plant Phys 41 (1990) 255-276.

[100] I. Enami, M. Kitamura, T. Tomo, Y. Isokawa, H. Ohta, S. Katoh, Is the Primary Cause of Thermal Inactivation of Oxygen Evolution in Spinach PS II Membranes Release of the Extrinsic 33 kDa Protein or of Mn, Bba-Bioenergetics 1186 (1994) 52-58.

[101] T. Miura, J.R. Shen, S. Takahashi, M. Kamo, E. Nakamura, H. Ohta, A. Kamei, Y. Inoue, N. Domae, R. Takio, K. Nakazato, Y. Inoue, I. Enami, Identification of domains on the extrinsic 33-kDa protein possibly involved in electrostatic interaction with photosystem II complex by means of chemical modification, J. Biol. Chem. 272 (1997) 3788-3798.

[102] N. Lydakis-Simantiris, R.S. Hutchison, S.D. Betts, B.A. Barry, C.F. Yocum, Manganese stabilizing protein of photosystem II is a thermostable, natively unfolded polypeptide, Biochemistry 38 (1999) 404-414.

[103] J.J. Pueyo, M. Alfonso, C. Andres, R. Picorel, Increased tolerance to thermal inactivation of oxygen evolution in spinach Photosystem II membranes by

substitution of the extrinsic 33-kDa protein by its homologue from a thermophilic cyanobacterium, Bba-Bioenergetics 1554 (2002) 29-35.

[104] K. Ifuku, T. Nakatsu, R. Shimamoto, Y. Yamamoto, S. Ishihara, H. Kato, F. Sato, Structure and function of the PsbP protein of Photosystem II from higher plants, Photosynth Res 84 (2005) 251-255.

[105] M. Tomita, K. Ifuku, F. Sato, T. Noguchi, FTIR Evidence That the PsbP Extrinsic Protein Induces Protein Conformational Changes around the Oxygen-Evolving Mn Cluster in Photosystem II, Biochemistry 48 (2009) 6318-6325.

[106] C.A. Kerfeld, M.R. Sawaya, H. Bottin, K.T. Tran, M. Sugiura, D. Cascio, A. Desbois, T.O. Yeates, D. Kirilovsky, A. Boussac, Structural and EPR characterization of the soluble form of cytochrome c-550 and of the *psbV2* gene product from the cyanobacterium *Thermosynechococcus elongatus*, Plant Cell Physiol. 44 (2003) 697-706.

[107] Y. Nishiyama, D.A. Los, H. Hayashi, N. Murata, Thermal protection of the oxygen-evolving machinery by PsbU, an extrinsic protein of photosystem II, in *Synechococcus species* PCC 7002, Plant Physiol. 115 (1997) 1473-1480.

[108] Y. Nishiyama, D.A. Los, N. Murata, PsbU, a protein associated with photosystem II, is required for the acquisition of cellular thermotolerance in Synechococcus species PCC 7002, Plant Physiol. 120 (1999) 301-308.

[109] J. Berry, O. Bjorkman, Photosynthetic Response and Adaptation to Temperature in Higher-Plants, Annu Rev Plant Phys 31 (1980) 491-543.

[110] M. Mamedov, H. Hayashi, N. Murata, Effects of Glycinebetaine and Unsaturation of Membrane-Lipids on Heat-Stability of Photosynthetic Electron-Transport and Phosphorylation Reactions in Synechocystis Pcc6803,

Biochim. Biophys. Acta 1142 (1993) 1-5.

[111] M. Havaux, F. Tardy, Temperature-dependent adjustment of the thermal stability of photosystem II in vivo: Possible involvement of xanthophyll-cycle pigments, Planta 198 (1996) 324-333.

[112] D. Nash, M. Miyao, N. Murata, Heat Inactivation of Oxygen Evolution in Photosystem II Particles and Its Acceleration by Chloride Depletion and Exogenous Manganese, Biochim. Biophys. Acta 807 (1985) 127-133.

[113] I. Enami, M. Kamo, H. Ohta, S. Takahashi, T. Miura, M. Kusayanagi, S. Tanabe, A. Kamei, A. Motoki, M. Hirano, T. Tomo, K. Satoh, Intramolecular cross-linking of the extrinsic 33-kDa protein leads to loss of oxygen evolution but not its ability of binding to photosystem II and stabilization of the manganese cluster, J. Biol. Chem. 273 (1998) 4629-4634.

[114] Y. Yamane, Y. Kashino, H. Koike, K. Satoh, Effects of high temperatures on the photosynthetic systems in spinach: Oxygen-evolving activities, fluorescence characteristics and the denaturation process, Photosynth Res 57 (1998) 51-59.

[115] N. Murata, S. Takahashi, Y. Nishiyama, S.I. Allakhverdiev, Photoinhibition of photosystem II under environmental stress, Biochim. Biophys. Acta 1767 (2007) 414-421.

[116] A. Yamashita, N. Nijo, P. Pospisil, N. Morita, D. Takenaka, R. Aminaka, Y. Yamamoto, Quality control of photosystem II: reactive oxygen species are responsible for the damage to photosystem II under moderate heat stress, J. Biol. Chem. 283 (2008) 28380-28391.

[117] P.G. Thomas, P.J. Dominy, L. Vigh, A.R. Mansourian, P.J. Quinn, W.P. Williams, Increased Thermal Stability of Pigment Protein Complexes of Pea Thylakoids Following Catalytic Hydrogenation of Membrane Lipids, Biochim. Biophys.

Acta 849 (1986) 131-140.

[118] Y. Murakami, M. Tsuyama, Y. Kobayashi, H. Kodama, K. Iba, Trienoic fatty acids and plant tolerance of high temperature, Science 287 (2000) 476-479.

[119] M. Alfonso, I. Yruela, S. Almarcegui, E. Torrado, M.A. Perez, R. Picorel, Unusual tolerance to high temperatures in a new herbicide-resistant D1 mutant from *Glycine max* (L.) Merr. cell cultures deficient in fatty acid desaturation, Planta 212 (2001) 573-582.

[120] M. Alfonso, R. Collados, I. Yruela, R. Picorel, Photoinhibition and recovery in a herbicide-resistant mutant from *Glycine max* (L.) Merr. cell cultures deficient in fatty acid unsaturation, Planta 219 (2004) 428-439.

[121] Y. Yamauchi, Y. Sugimoto, Effect of protein modification by malondialdehyde on the interaction between the oxygen-evolving complex 33 kDa protein and photosystem II core proteins, Planta 231 (2010) 1077-1088.